Structure of Bolaamphiphile Sophorolipid Micelles Characterized with SAXS, SANS, and MD Simulations

Sabine Manet, Anne-Sophie Cuvier, Claire Valotteau, Giulia C. Fadda, Javier Perez, Esra Karakas, Stéphane Abel, Niki Baccile

Structure of Bolaamphiphile Sophorolipid Micelles Characterized with SAXS, SANS and MD Simulations

*Sabine Manet,[1] Anne-Sophie Cuvier,[1] Claire Valotteau,[1] Giulia C. Fadda,[2] Javier Perez,[3] Esra Karakas,[4,5] Stéphane Abel,[5] and Niki Baccile[1]**

[1] Sorbonne Universités, UPMC Univ Paris 06, CNRS, Collège de France, UMR 7574, Chimie de la Matière Condensée de Paris, F-75005, Paris, France.
[2] Laboratoire Léon Brillouin, LLB, CEA Saclay, F-91191 Gif-sur-Yvette Cedex, France
[3] SWING, Synchrotron Soleil, BP 48, F-91192 Gif-sur-Yvette
[4] Maison de la Simulation, USR 3441, CEA – CNRS – INRIA – Univ. Paris-Sud – Univ. de Versailles, 91191, Gif-sur-Yvette Cedex, France
[5] Institute for Integrative Biology of the Cell (I2BC), Commissariat à l'Energie Atomique et aux Energies Alternatives (CEA), Centre National de la Recherche Scientifique (CNRS), Université Paris-Sud, CEA-Saclay, F-91191 Gif-sur-Yvette, France

* Corresponding author : Laboratoire de Chimie de la Matière Condensée de Paris, Collège de France, 11, Place M. Berthelot, F-75005, Paris, France. Tel. +33 1 44 27 15 44 ; Email : niki.baccile@upmc.fr

Abstract

The micellar structure of sophorolipids, a glycolipid bolaamphiphile, is analyzed using a combination of Small Angle X-ray Scattering (SAXS), Small Angle Neutron Scattering (SANS) and Molecular Dynamics (MD) simulations. Numerical modeling of SAXS curves shows that micellar morphology in the non-charged system (pH< 5) is made of prolate ellipsoids of revolution with core-shell morphology. Opposed to most surfactant systems, the hydrophilic shell has a non-homogeneous distribution of matter: the shell thickness in the axial direction of the ellipsoid is found to be practically zero, while it measures about 12 Å at its cross-section, thus forming a "coffee bean" like shape. The use of contrast matching SANS experiment shows that the hydrophobic component of sophorolipids is actually distributed in

a narrow spheroidal region in the micellar core. These data seem to indicate a complex distribution of sophorolipids within the micelle, divided into at least three domains: a pure hydrophobic core, a hydrophilic shell and a region of less defined composition in the axial direction of the ellipsoid. To account for these results, we make the hypothesis that sophorolipid molecules acquire various configurations within the micelle including bent and linear, crossing the micellar core. These results are confirmed by MD simulations which do show the presence of multiple sophorolipid configurations when passing from spherical to ellipsoidal aggregates. Finally, we also used Rb^+ and Sr^{2+} counterions in combination with Anomalous SAXS experiments to probe the distribution of the COO^- group of sophorolipids upon small pH increase ($5 < pH < 7$), where repulsive intermicellar interactions become important. The poor ASAXS signal shows that the COO^- groups are rather diffused in the broad hydrophilic shell rather than at the outer micellar/water interface.

Keywords

Self-assembly; Biosurfactants; Glycolipid; *Starmerella bombicola*; ASAXS; Bolaform

Introduction

Surfactants are compounds employed in a very large panel of applications in which amphipathic interfaces are made compatible. The formation of micelles above a critical micellar concentration is one of the most common aspects among amphiphilic molecules in water and a thorough description of their structure is one of the first steps when studying the properties of new compounds.[1] If the aggregation of classical cationic (e.g., alkylammonium salts),[2-4] anionic (e.g., alkylsulfates salts) or non-ionic (e.g., block copolymers)[5] surfactants into micelles has been studied, both experimentally and theoretically, for decades, less conventional compounds are much less looked at. Among these, bolaform lipids[6] constitute a class of interesting molecules with two functional end-groups. If the end-groups are chemically equivalent, one speaks of symmetric bolaamphiphiles (bolas), otherwise one refers to asymmetric bolas. The atypical distribution of amphiphilic and lypophilic regions within the same molecule is often responsible of interesting aggregation phenomena which lead to the formation of micelles, bicelles,[7] vesicles,[8] cones,[9] fibers,[10] tubes,[11,12] etc... Many significant systems have been reviewed in 2004 by Fuhrhop,[6] while Fariya *et al.*[13] have recently reviewed bolaamphiphiles in the context of pharmaceutical applications. If a large amount of work has been dedicated to the synthesis and characterization of bola systems, much less has been devoted to a thorough structural study. In the context of micellar objects

composed of bolaamphiphiles,[8,10,14- 20] advanced structural considerations of the micellar packing and bola distribution are rare.[19.20] Indeed, Nagarajan[21] predicted since 1987 the formation and structure of micelles composed of bolaamphiphiles basing his hypotheses on the analysis of the packing parameter. Interestingly, he predicted the formation of spherical, cylindrical and discoidal micelles, in which he imagined that the bolaform compound has various configurations: elongated, which induces transradial crossing of the end-groups; folded, under which the end-groups lie both on the same side. If Yan *et al*.[14] have proceeded with macroscopical verification of Nagarajan's assumptions by observing a pH/cosolvent-driven tube-to-vesicle-to-micelle transition in disodium phenyl-1,4-bis(oxyhexanoate) solutions, the actual bola distribution within the micelle was never elucidated. Additional insights in the structural composition of bola-composed micelles have been discussed in Ref. 7,14-20 mainly using Small Angle Neutron Scattering (SANS) and/or self-diffusion Nuclear Magnetic Resonance (NMR) experiments. However, in practically all cases, these experiments have been used to describe the micellar shape and size. Only few authors, with little consensus in their conclusions, have tried to determine the molecular distribution of the bolaamphiphile within the micellar aggregate. Caponetti *et al*.[16], for instance, have used advanced modelling analyses of SANS spectra to study the bola *N*-aza-18-crown-6 ether compound. If Davey *et al*.[19] and Shinde *et al.*[20] agree on the fact that their respectively studied asymmetric bolaamphiphiles, alcohol derivatives of alkylammonium and oleate salts, form uniform spherical/cylindrical micelles in which both polar groups are in contact with the solvent (water), they do not agree on the molecular arrangements. Davey proposes an elongated cross-micellar conformation, while Shinde proposes a bent configuration. Interestingly, these recent studies disagree with older works in which it was proposed that only one of the two polar groups is actually located at the micellar/solvent palisade.[22,23]

Such a lack of deep characterization of bola-micelles, and disagreement on their structure and molecular conformation, is quite odd because of the importance in terms of applications for many bola systems. In fact, the chemical nature of end-groups in bolas can be as wide as imagination can allow: polymerizable,[24] complexing,[16,25] pH-responsive,[11,14] fullerenic,[26] chiral,[27] glycosidic,[18] functions are just some examples of the broad variety that one can find in the literature. The range of applications of bolas in general goes from one-pot porous material synthesis[24] to supramolecular materials with temperature-driven ferroelectric-paraelectric transitions,[25] ion-channel supramolecular membranes,[28] metallo-hydrogels for dye adsorption and water purifier,[16,29] viscoelastic fluids,[30] biomedical carriers[13] and much more. For this reason, it is of paramount importance to characterize the spatial distribution

and accessibility of end-functions within the supramolecular aggregates and, in particular, within micelles. Laying one of the end-groups within the interior of the micellar aggregate can be of relevance for drug-delivery systems and conception of nanoreactors. Whether charged end-groups concentrate at the micellar surface or not can be of relevance in nanomaterial synthesis procedure in which charge matching drives the material formation, such as mesostructured oxides or layer-by-layer approaches, but it can also have drastic relevance in gelling properties, for instance. The distribution and accessibility of biologically-relevant moieties like peptides or carbohydrates is important for biomedical applications like gene-antigene recognition for cancer treatment. Even in the system studied by Caponetti,[16] in which authors looked at metal-binding affinity of the crown ether end-groups, it is necessary to know the distribution of the crown ether groups and their accessibility in view of metal ion removal in solution.

For these reasons, in the present work, we try to set up a combination of complementary analytical approaches based on advanced small angle scattering techniques in order to prove both indirectly (by way of model functions) and directly the spatial distribution of a glycolipid asymmetric bolaamphiphile. We study here the micellar structure of sophorolipids, a yeast-derived bolaform glycolipid composed of sophorose (glucose β(1,2)) attached to the C17 atom of oleic acid *via* an ether bond, the carboxylic group being free of access at the opposite side of the molecule (Figure 1).[31] This compound is part of the glycolipid family and the presence of sophorose-COOH end-groups make it, *de facto*, a bolaform compound with pH-responsive properties,[32] which confer to it a double neutral/anionic or neutral/neutral nature.[33] Recent works on the self-assembly of the acidic open chain form of sophorolipids have shown its ability to form assemblies such as fibers[34,35] and micelles.[32,36] In the latter case, our group has shown that the micellar charge can be adjusted using pH.[33] However, no information on the charge distribution could be obtained. Considering the fact that this compound is easily accessible and considering its importance in various fields like detergency,[37] cosmetics,[38] nanoscience,[39] disinfection,[40] medicine,[41] it becomes a valuable candidate to use for a detailed study of the sophorose/COOH end-groups distribution within the micelle. To do so, we combine several small-angle scattering techniques: Small Angle X-ray Scattering (SAXS) is used to precisely define the micellar morphology and its size; Anomalous-SAXS (ASAXS), a technique that probes the distribution of counterions around a charged macroion, is employed to follow the distribution of the carboxilate end-group in the presence of specific ASAXS probe counterions, Rb^{+} and Sr^{2+}; contrast matching Small Angle Neutron Scattering (SANS) is used to visualize the

distribution of the hydrophobic fraction of the molecule. This approach shows that, in the mild acidic pH region (pH< 5), the micelle is likely to be described as an ellipsoid of revolution having a “coffee bean” like morphology. In this structure, the hydrophobic region only occupies a small inner spheroidal core. The outer shell in the central region of the ellipsoid is mainly made of sophorose and COOH groups. The electron density distribution in the axial direction is more difficult to define and it probably reflects a more complex distribution of matter. We identify at least two different configurations of the sophorolipid molecules: bent and elongated, with possibility of crossing the ellipsoid section. We also show that these hypotheses, based on experimental work, are confirmed by Molecular Dynamics (MD) simulations specifically performed in this work. Upon formation of COO^- groups in the neutral pH range (5 < pH < 7), micelles become negatively charged: ASAXS experiments seem to indicate that the carboxylates are rather diffused in the broad hydrophilic shell rather than localized at the micelle/solvent palisade. To the best of our knowledge, such a complex analysis has never been carried neither on glycolipid-based nor on any other bolaamphiphile compound.

Experimental

Acidic sophorolipids (SL) have been prepared from a commercial batch of a sophorolipid mixture (Sopholiance, Soliance, France; sophorolipids are derived from rapeseed oil, batch number: 11103A, dry content: 60 ± 6 %) using alkaline hydrolysis to convert the lactonic/acidic mixture into a fully acidic sophorolipid compound. Extraction and purification have been performed using the method N°2 described in ref. 42, to which one should refer for a typical ^1H solution NMR spectrum of the compound used. As a general observation on purity, one should note that our compound has a very low content of residual fatty acids (typically less than 5 mol% by ^1H NMR). Nevertheless, biobased glycolipids in general are known to contain residual congeners. In the case of sophorolipids, mainly composed of a C18:1 fatty acid tail attached to sophorose, congeners generally represent a low fraction of the actual compound, generally being C16 and/or C18:2 fatty acids variations. A typical HPLC chromatogram was reported in ref. 43, showing that C18:1 does constitute the large majority of our sample (> 90 %), thus being in agreement with the ^1H NMR data. Congeners are also detected but in the present work we make the hypothesis that, given the low amount, their influence on the self-assembly of C18:1 sophorolipid is negligible.

Sophorolipid solutions are generally prepared by simply dispersing the compound in water (50 mg/mL ≡ 80 mM). If needed, a slightly warm (30-35°C) ultrasonic bath is used for few

seconds to help solubilize the sample. After solubilization, the solutions are clear and stable over time. Specific sample preparation is detailed in each sub-section below. MilliQ quality water was used for the experiments and all solutions are freshly prepared. RbCl, $SrCl_2$, RbOH and $Sr(OH)_2$ have been purchased at Sigma-Aldrich.

Small Angle X-ray Scattering (SAXS). The sample composition is presented in Table 1 and for all of them the concentration of SL is 50 mg/mL. Rb^+ and Sr^{2+} have been used instead of the more classical Na^+ and Ca^{2+} ions due to their activity in the ASAXS experiments, presented later. Each sample is prepared by mixing the salt in water; this solution is eventually split in half, one half is used for background acquisition and the indicated amounts of SL are introduced in the second half.

Table 1 – List of samples studied in this work. Sophorolipid concentration is constant (80 mM) for all samples

Sample	Compound	[Sr^{2+}] mM	[Rb^+] mM
1	**RbCl**	-	10
2	**RbCl**	-	50
3	**RbCl**	-	100
4	**RbOH**	-	40
5	**RbOH**	-	80
6	**$SrCl_2$**	5	-
7	**$SrCl_2$**	25	-
8	**$SrCl_2$**	50	-
9	**$Sr(OH)_2$**	10	-
10	**$Sr(OH)_2$**	20	-

These experiments have been done at the SWING beamline of the SOLEIL synchrotron at Saint-Aubin (France). Sample-to-detector distance was set to 2526 mm and energy of the X-ray beam was E= 14.6 keV. The experimental environment was provided at the beamline and consisted of a flow-through quartz capillary which it was possible to fill using a syringe. The X-ray beamline hits the same capillary position, which does not change between background and sample acquisitions, thus making the background subtraction highly accurate. For the background, we used the same solution used to prepare a given sophorolipid sample, as also mentioned above. Absolute scaling was calibrated on the signal of water. All data have been divided by the sample transmitted intensity. Data treatment (mask generation, integration) was done using the Foxtrot software provided at the beamline.

Modelling SAXS data.

The analysis of the SAXS profiles for the determination of micelle size and shape parameters has been made with the models displayed by default in the SASview software, provided free of charge on the developer's website.[44] The general equation treating the scattered intensity versus the momentum transfer q is (Eq. 1)

$$I(q) = \frac{scale}{V}\left(\rho - \rho_{solv}\right)^2 P(q)\, S(q) + bkg \qquad \text{Eq. 1}$$

where, *scale* is the volume fraction, *V* is the volume of the scatterer, ρ is the scattering length density (SLD) of the object, ρ_{solv} is the SLD of the solvent, *P(q)* is the form factor of the object, *S(q)* is the structure factor and *bkg* is a constant accounting for the background level.

Form factor

The analytical expressions of the P(q) discussed below are directly implemented in the SASview software and their analytical form is provided in Ref. 45. The $\chi 2$ test is employed to characterize the quality of the fit, the lower value indicating the best fit. χ^2 is defined as the Pearson's cumulative test statistic, $\chi^2 = \sum_{i=1}^{Npts} \frac{(O_i - E_i)^2}{E_i}$, where O_i is an observed measured value; E_i is an expected (theoretical) value, asserted by the null hypothesis. The χ^2 is then normalized by the number of points in the distribution, $\chi^2/Npts$. Some fit parameters can be simply estimated from the sample composition and have been fixed for the fitting process. Among them, the volume fraction of scattering objects has been set at 0.05, reflecting the SL mass concentration of 50 mg/mL (80 mM) used for all samples.

The core and solvent SLD's have been fixed and calculated using Eq. 2:

$$\rho = \frac{\sum_i^j Z_i r_e}{V_M} \qquad \text{Eq. 2}$$

where Z_i is the atomic number of the i^{th} of j atoms in a molecule of molecular volume V_M and r_e is the classical electron radius or Thomson scattering length (2.8179 x 10^{-15} m). Sophorolipids are mainly composed of a C18 aliphatic chain with one unsaturated C=C bond (position $C_{9,10}$), one COOH group (position C_1), the CH in position C_{17} covalently bonded to sophorose and a CH_3 in position C_{18} (Figure 1). Considering the fact that C_{17} and C_{18} atoms are located at the sophorose/aliphatic frontier, it is a difficult choice to decide which is their exact location. For this reason, we simplify our model and make the assumption that the hydrophobic core starts at the C_{16} carbon, neglecting the contribution of the C_{17} and C_{18} positions. Under these conditions, we define the molecular volume, V_M, of the hydrocarbon

chain to be $13V_{CH_{2,mic}}$ + $2V_{CH}$, where $V_{CH_{2,mic}}$ is the volume of one CH_2 group inside a micelle, 27.5Å^3, and V_{CH} is the volume of a CH group, 22.0Å^3.[46] These estimations provide a SLD core value, constant for all fitting procedures in this study, of 8.3 x 10^{-6} Å^{-2} (294 e^-/nm^3). The solvent SLD has been calculated taking into account the salt or base concentration influencing the molecular volume.[47] The resulting SLD values are very close and lie between 9.4 and 9.5 x 10^{-6} Å^{-2}, (334 and 337 e^-/nm^3, see full list in Table S1 in the Supporting Information). For core-shell models, the shell SLD is always a variable parameter. We make the hypothesis that the shell is most likely composed of hydrated sophorose; in this case, the shell SLD value should lie between the solvent and hydrated sophorose SLD values, roughly between 1.0 and 1.2 x 10^{-5} Å^{-2}, (355 to 425 e^-/nm^3). As a result, the electron density profile from the center of the micelle to the solvent can be drawn as a hat-like shape, in which the shell SLD is the highest value. The choice of the form factor has been determined by comparing the best fits on the basis of the lowest $\chi^2/Npts$ among different model functions, as critically discussed on Page S2 in the Supporting Information and shown in Figure S1. We find that a core-shell prolate ellipsoid of revolution, schematized in Figure 2, best describes our SAXS data.

Structure Factor

The structure factor, *S(q)*, which quantifies the intermicellar interactions/correlations, is included in our fitting process using the "Hayter-MSA-Structure" model displayed in the SASview software. This accounts for a repulsive screened Coulombic intermicellar interaction potential,[48,49] as previously used on similar systems.[33] *S(q)* has only been used for samples containing RbOH (samples 4,5) and $Sr(OH)_2$ (samples 9,10) according to the previously discussed assumption that deprotonation of the COOH introduces negative charges at the micellar/solvent palisade,[33] thus being responsible of the broad interaction peak observed in small angle neutron scattering spectra, and reproduced in this work. *S(q)* has been set equal to 1 for base-free samples only containing salts (samples 1-3 and samples 6-8 in Table 1). Six parameters are needed to compute the Hayter and Penfold structure factor: the dielectric constant, the volume fraction, the effective radius of interacting objects, the temperature, the surface charge of the micelle, and the salt concentration, used to calculate the ionic strength of the solution, which in turn is used to compute the Debye screening length. As this model is made for monovalent ions, we modified the salt concentration parameter of the samples, otherwise fixed and equal to the experimental concentration, with divalent ions

so that the resulting Debye length is correct. The volume fraction of the scatterers is calculated from V_{mic} and n_{mic} ($\eta = V_{mic} n_{mic}$), defined more precisely later on in this same section, and inserted in the Hayter-MSA-Structure routine with R_E, effective radius of interacting objects ($R_E = \frac{1}{2}\left(\frac{6\eta}{\pi n_{mic}}\right)^{1/3}$, see Ref. 48) as fixed parameters. The temperature, dielectric constant and salt concentration are also fixed parameters so that the micelle charge is the only refinable parameter for the calculation of *S(q)*.

Fit strategy using a core shell prolate ellipsoid of revolution model and a Hayter-MSA structure factor

In order to reduce the number of parameters used for the fitting process, we used a customized version of the core-shell prolate ellipsoid form factor proposed in the 3.0.0 version of SASview. In particular, we introduce some molecular constraints inspired by the work of Hayter and Penfold.[4] By making some assumptions described thereafter, only 5 fitting parameters are needed: N_{agg} (aggregation number), R_C (equatorial core radius, see Figure 2), ρ_S (scattering length density of the shell, see Figure 2), X_C (axial core ratio, see Figure 2) and *z*, the surface charge of the micelle. A small background correction (<0.005 cm^{-1}) has also been applied. In the Hayter and Penfold model, if N_{agg} is greater than the one expected to accommodate a sphere, the radius of which is $R_c = l_c$ (length of the fully extended hydrocarbon chain of the surfactant), then the object is allowed to become elliptical so to accommodate the molecular excess. This model has been adapted to the sophorolipid surfactants as follows. For a given N_{agg}, the spherical hard core micelle radius R_{hc} is defined as:

$$R_{hc} = \left[\frac{3N_{agg}\left(13V_{CH_{2,mic}} + 2V_{CH}\right)}{4\pi}\right]^{1/3} \qquad \text{Eq. 3}$$

If $R_{hc} > l_c$, R_C is set to l_c, and a parameter α is introduced, defined as the fraction of CH_2 inserted in the dry core of the micelle :

$$\alpha = \frac{V_C - 2V_{CH}}{N_{agg}\,13V_{CH_{2,mic}}} \qquad \text{Eq. 4}$$

with $V_C = \frac{4}{3}\pi R_C^{\,3}$. If $R_{hc} < l_c$, R_C is set to R_{hc} and $\alpha = 1$.

Sophorolipids are bolaform amphiphiles with two different polar heads (carboxylic acid and sophorose sugar moiety) connected to a 18:1 carbons lipid chain (Figure 1), which reduces to a C16:1 chain if one makes the hypothesis that C_{17} (CH) and C_{18} (CH_3) do not contribute to l_c, which in this case can be estimated to be around 10 Å, half the length of the 16 carbons chain. We first try to use this value of l_c as R_{test}, but the results obtained were not reliable, leading to high $\chi^2/Npts$ values, so we let this constraint to relax, and R_C and X_C have been set as refinable parameters. Recently, Penfold *et al.*[36] have made the same choice when analyzing the SANS profiles of sophorolipid micelles, arguing that the particular alkyl chain geometry of the sophorolipid introduces some uncertainty into what value the inner radius should be constrained to.

Once α is known, the number of water molecules per sophorolipid in the shell, $n_{w/SL}$, and consequently the composition of the shell, can be calculated using the shell scattering length density ρ_S as a refinable parameter, assuming that the shell hydration should not be a fixed parameter, because it depends on many effects like the number of hydrated CH_2 or the micelle surface charge. From Eq. 5 we calculate the molar volume, $V_{m,hg}$, and hence the SLD, ρ_{hg}, of the total dry headgroup. Composition of the dry headgroup is not easy to estimate; it certainly includes sophorose, as stated earlier, and most likely the COOH group, but it can also include the C_{17} (CH) and C_{18} (CH_3) atoms, previously excluded from the core region of the micelle, as well as the fraction of the CH_2 aliphatic chain excluded by the α parameter presented in Eq. 4. This is not surprising as hydration of the CH_2 groups close to the hydrophilic head was reported before both experimentally[50,51] and predicted theoretically using MD simulation[52]. In all cases, the ionic species coming from the added salts or bases are neglected. The general expressions for the headgroup volume and SLD are then:

$$V_{m,hg} = \sum_i V_i + 13(1-\alpha)V_{CH_{2,w}} \qquad \text{Eq. 5}$$

$$\rho_{hg} = \frac{\sum_i \rho_i V_i + 13(1-\alpha)\rho_{CH_{2,w}} V_{CH_{2,w}}}{V_{m,hg}} \qquad \text{Eq. 6}$$

where *i* denotes the sophorose, carboxylate and the aliphatic moieties, CH, CH_3 and possibly CH_2 groups. $V_{CH_{2,w}}$ is the molar volume of hydrated CH_2 smaller than $V_{CH_{2,mic}}$, taken as 26.7Å^3,[53] while $\rho_{CH_{2,w}}$ is the SLD of the hydrated CH_2. The volume fraction of water in the

shell $x_{v,w}$ and the number of water molecules per sophorolipid in the shell $n_{w/SL}$ are obtained by considering the fraction of water molecules ($n_{w/SL}$) needed to equalize the calculated ρ_{hg} (Eq. 6) and the experimental ρ_{shell} (obtained from the fit). This is summarized in Eq. 7 and Eq. 8:

$$x_{v,w} = \frac{\rho_{shell} - \rho_{hg}}{\rho_w - \rho_{hg}} \qquad \text{Eq. 7}$$

$$n_{w/SL} = \frac{x_{v,w} V_{m,hg}}{(1 - x_{v,w}) V_{m,w}} \qquad \text{Eq. 8}$$

with $V_{m,w}$ the molar volume of water (29.9 Å^3) and ρ_w the water SLD taken as 9.4 x 10^{-6} Å^{-2}. As it did not seem straightforward to evaluate the ionic composition and concentration within the shell, the presence of ions coming from added salts, acid or base has been neglected. However, the same fitting process applied using ρ_{solv} instead of ρ_w in Eq. 7 did not show a deep impact of the ionic composition of the shell on the results (results not shown).

The total micelle volume V_{mic} is then calculated as the sum of all the components in the core and in the shell:

$$V_{mic} = N_{agg}\left(13\alpha V_{CH_2,mic} + 2V_{CH} + V_{m,hg} + n_{w/SL} V_{m,w}\right) \qquad \text{Eq. 9}$$

As V_{mic} can also be defined as the volume of an ellipsoid described by the equatorial core radius R_c, the axial core ratio X_C, the axial shell ratio X_S (see Figure 2) and the equatorial shell radius R_S [$V_{mic} = \frac{4}{3}\pi R_S^2\left(R_C X_C + (R_S - R_C)X_S\right)$, see Figure 2], the latter geometric parameter can then be obtained as the real root of this polynomial equation:

$$X_S R_S^{\,3} + R_C\left(X_C - X_S\right)R_S^{\,2} - 3\frac{V_{mic}}{4\pi} = 0 \qquad \text{Eq. 10}$$

The core-shell prolate ellipsoid form factor is finally calculated by:

$$P(q) = n_{mic}\int_0^1 |F(q,\mu)|^2 d\mu + background$$

$$F(q,\mu) = V_C(\rho_C - \rho_S)\left[\frac{3j1(x_C)}{x_C}\right] + V_{mic}(\rho_S - \rho_{solv})\left[\frac{3j_1(x_S)}{x_S}\right] \qquad \text{Eq. 11}$$

$$j_1(x) = \frac{sinx - xcosx}{x^2} \quad \text{Eq. 12}$$

$$x_C(q,\mu) = q\left(R_C{}^2 X_C{}^2 \mu^2 + R_C{}^2 \left(1-\mu^2\right)\right) \quad \text{Eq. 13}$$

$$x_S(q,\mu) = q\left(R_S{}^2 X_C{}^2 \mu^2 + R_S{}^2 \left(1-\mu^2\right)\right) \quad \text{Eq. 14}$$

The intensity scattered by interacting micelles defined as $I(q) = n_{mic} P(q) S(q)$ can be calculated by relating the micelle density n_{mic} to the known sophorolipid surfactant concentration [SL] (80 mM) and the refinable aggregation parameter N_{agg}, with N_a being the Avogadro's number:

$$n_{mic} = \frac{[SL] N_a}{N_{agg}} \quad \text{Eq. 15}$$

Anomalous Small Angle X-ray Scattering (ASAXS).

Elements of theory. Extraction of the counterion scattering contribution around sophorolipid micelles was done via recording the anomalous scattering contribution of rubidium and strontium cations. The anomalous effect is measured when the energy of the X-ray beam approaches the absorption edge of a given element. In this case, the scattering factor becomes a complex function and it is no more a constant. The contribution of the scattering factor far from the absorption edge is

$$f_{ion} = f_0 - \rho_m V_{ion} \quad \text{Eq. 16}$$

where f_0 equals the atomic number of the element, ρ_m is the electron density of water and V_{ion} is the volume of the counterion. Upon approaching of the edge, f_{ion} becomes

$$f_{ion} = f_0 - \rho_m V_{ion} + f'(E) + if''(E) \quad \text{Eq. 17}$$

where $f'(E)$ and $f''(E)$ are, respectively, the real and imaginary part of the energy-dependent scattering vector. Values for $f'(E)$ and $f''(E)$ are tabulated,[54,55] but they can also be calculated from the experimental absorption spectrum.[56] When approaching the absorption edge by tuning the synchrotron incident beam energy, f_{ion} is neither constant nor negligible anymore

and the scattered intensity must take that into account. The resulting general expression for the scattering intensity then becomes

$$I_0(q,E) = F_0^2(q) + 2f'(E)F_0(q)v(q) + \left[f'^2(E) + f''^2(E)\right]v^2(q) \qquad \text{Eq. 18}$$

where $F_0^2(q)$ is the nonresonant intensity of the macroion (= micelle, polymer, *etc*...) measured far from the absorption edge; $F_0(q)$ and $v(q)$ are the nonresonant and resonant amplitudes respectively of the macroion and the counterion; $v^2(q)$ is the pure resonant curve of the counterion measured at the absorption edge. A constant term due to fluorescence, affecting the intensity above the absorption edge, has been omitted. For a more extended discussion on the SAXS theory near the absorption edge of a given element, one can refer to references 57-59. From Eq. 18, one is generally interested into extracting the pure resonant curve $v^2(q)$, which gives the scattering profile of the counterion alone. Since $I_0(q,E)$ contains three independent variables, one cannot extract directly $v^2(q)$. Two complementary methods are proposed in the literature to operate in such a way. In all cases, one must record the $I_0(q,E)$ at various values of the incident beam energy, far and close to the absorption edge. The classical SAXS experiment described in the previous section must then be repeated by changing the value of E. The first method, called the "matrix" method, consists of a numerical solution of $I_0(q,E)$ needing at least three different energy values.[60] The second approach, called the "fit" (or "Ballauf") method,[61] consists of neglecting the $f''(E)$ term before the absorption edge and performing a quadratic interpolation of $I_0(E)$ for each value of the scattering vector. For a detailed discussion on the problem of solving $I_0(q,E)$, one can refer to Ref. 60-63. The experimental approach and data treatment used to treat our ASAXS experiments is detailed on Page S6 in the Supporting Information.

Contrast matching Small Angle Neutron Scattering (SANS). These experiments have been performed to look at the contribution of the micellar core only, thus matching the scattering of the sophorose headgroup (molecular formula: $C_{12}H_{21}O_{11}$, molar mass: 341.30 g/mol) in the simple ion-free sophorolipid micellar system at 80 mM. For the SLD calculations, we used the bulk sophorose density (1.68 g/mL)[64] and we considered the fact that labile COH groups could be exchange into COD. The estimated SLD for sophorose under these conditions is ~ 2.6 x 10^{-6} $Å^{-2}$, corresponding to a ~46:54 = D_2O:H_2O mixture. These values are to be considered as an approximation because the exact sophorose density in sophorolipid is not

exactly known. Two samples have then been prepared at concentration of the sophorolipid of 50 mg/mL: a) in fully deuterated water (100:0 = D_2O:H_2O) and b) in 46:54 = D_2O:H_2O mixture.

SANS experiments have been performed on the PACE beamline at the Laboratoire Léon Brillouin (LLB) facilities at CEA-Saclay (France). 1 mm quartz cells have been used as sample holder. The low-q portion of the data was recorded using a sample-to-detector distance of 4565.95 mm and wavelength of 6 Å while the high-q portion was recorded using 866.14 mm and 6 Å. The scattering intensity is obtained from the determination of the number of neutrons in the incident beam and the detector cell solid angle. Data were corrected for the ambient background, empty cell scattering, neutron beam transmission and detector efficiency and normalized to the neutron beam flux to get the scattered intensity I(q) in absolute units according to ref. 65. Incoherent signal was substrated by measuring the background value at high-q values for both, sample-free, 100:0 = D_2O:H_2O and 46:54 = D_2O:H_2O mixtures. All data have been treated using the Pasinet 2 software[66] provided at the beamline free of charge. Pair distribution function analysis, P(r), was done using the SASView software package[44] using estimated Dmax values of 40 Å and 140 Å, respectively for the 46:54 and 100:0 = D_2O:H_2O mixtures.

Molecular dynamics simulations.

All the MD simulation discussed in this paper were carried out with GROMACS (v4.6.6)[67,68] and with the protonated acidic sophorolipid (SL) molecule presented in Figure 1. Since the SL ionization degree is found to be < 5 % (see the experimental section) and similar to Prasad *et al.*,[69] we only simulated the protoned form of the SL and without ions. As in a previous work[69] to model the surfactant, we used an "united-atom" force field based on the GROMOS53A6[70]. In particular, the parameters of the sophorose group were taken from the GROMOS53A6 force field for carbohydrates (56A6$_{CARBO}$) developed by Hansen *et al.*[71] Concerning the alkyl chain (with the double bond) and the COOH groups, the parameters were taken from Kukol[72] and the glutamic acid parameters available in the GROMOS53A6[70] force field, respectively. To be consistent with the GROMOS force field, we used the simple charge water model (SPC)[73] to model water with the SETTLE algorithm[74] to keep its geometry rigid.

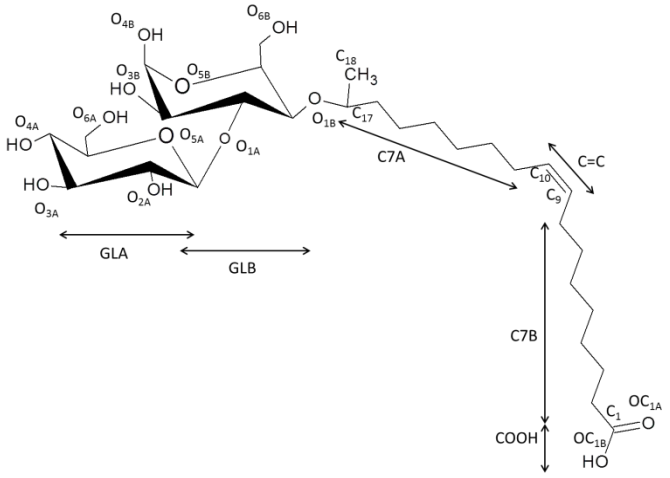

Figure 1 - Acidic sophorolipid surfactant with the atom-numbering scheme and part used in the work (see main text for details).

We have to mention that by not taking into account in the simulation the effects of the pH and presence of the ions in the solution, our simulations may have some limitations. However, as we will see further, the simulation results are consistent with the reported experimental data and we think they provide a good model basis of the micelle as a function of their aggregation numbers. To have a large overview of the micelle characteristics as a function of the SL aggregation number, N_{agg}, we carried out 6 MD simulations with different SL N_{agg} values (Table 2). Specifically, we chose 28 and 37, values obtained by Penfold *et al.*[36] for mixture of sophorolipids (sample S4 in ref. 36: 52.2% non acetylated, 39% mono-acetylated and 8.5% di-acetylated) respectively at 5 mM and 30 mM; 56 and 68 adapted from the SAXS data in this work (Table 3, RbCl system). In addition to these simulations, we also performed two more simulations with N_{agg} = 80 and 112, to examine the effect of high N_{agg} values of the SL aggregate structure. These two N_{agg} values correspond to an intermediary point between 56 and 68 and a value estimated by Penfold.[36] The effective concentrations of the simulated systems are in a range of 110 mM and 456 mM (given SL mass fraction, SL wt% of 6.2 – 12.6 %), larger than the experimental concentration (80 mM) to reduce the number of water molecules and, consequently, the computational cost of the simulations. To construct the system for simulation, we used a *self-assembled* approach, where the corresponding number of sophorolipids with a random orientation was inserted in a SPC water cubic box. All the systems were minimized, equilibrated and finally simulated at ambient conditions (P = 1.015 bar and T = 303 K). Specifically, the temperature and the pressure were controlled with the Bussi *et al.*[75] thermostat (τ_T = 0.1 ps) and the Parrinello-Rahman[76,77] barostat (τ_p = 3.0 ps and with a compressibility of 45 x 10^{-6} bar^{-1}). During the

equilibration stages, the SL molecules were harmonically restrained with a force constant of 1000 kJ.mol.nm^{-1} to equilibrate the solvent around the sophorolipids. SL and water molecules were coupled separately with two thermostatic baths as a standard rule. To integrate the equations of motions, we used a time step of 2 fs with the P-LINCS algorithm[78] to restrain bond lengths to their equilibration values. Electrostatic interactions were treated with the reaction field approach[79] with the non-bonded interactions evaluated with a twin range cutoff scheme, with a short- and long-range cutoff distances of 8 Å and 14 Å, respectively and an update frequency of 2 timesteps for the short-range pair list. To correct the truncation of electrostatic interactions outside the cutoff of 14 Å, a reaction field term[79] corresponding to a relative dielectric permittivity of the SPC water (61)[80] was added. Finally, the production simulations were performed during 110 – 162 ns with the atomic data collected every 2 ps for subsequent analysis

Table 2 - Overview of the simulated systems. N_{agg}, n_{H2O} and n_{atom} are the numbers of sophorolipid monomers, water, and atoms composing each systems. n_{Water}/SL, SLwt% [SL], L_{box} and t_{sim} are the number of water per sophorolipid molecule, the sophorolipid concentration, the total mass fraction, the box size and the simulation time (in ns), respectively.

#MD	N_{agg}	n_{H2O}	n_{atom}	n_{Water}/SL	SLwt%	[SL] M	L_{box} (Å)	t_{sim} (ns)
MD1	28	13600	42228	485.7	6.6	0.114	76.3	112
MD2	37	18000	55887	486.5	6.6	0.114	77.7	110
MD3	56	13600	43656	242.9	12.4	0.228	83.7	162
MD4	68	16500	52968	242.6	12.4	0.228	82.9	164
MD5	80	19400	62280	242.5	12.4	0.228	87.5	162
MD6	112	13600	46512	121.4	22.0	0.456	80.4	144

Results and Discussion

Description of the "coffee bean" like prolate ellipsoid of revolution model

As critically discussed on Page S2 in Supporting Information, the best shape model to fit SAXS data is the core-shell prolate ellipsoid of revolution function, which gives good $\chi^2/Npts$ values below 15. The geometric parameters of this model are the equatorial core radius, R_C, the axial core ratio X_C (X_C>1 for prolate micelles), the equatorial shell thickness, T_S, and the polar shell ratio in the axial direction, X_S (see Figure 2).

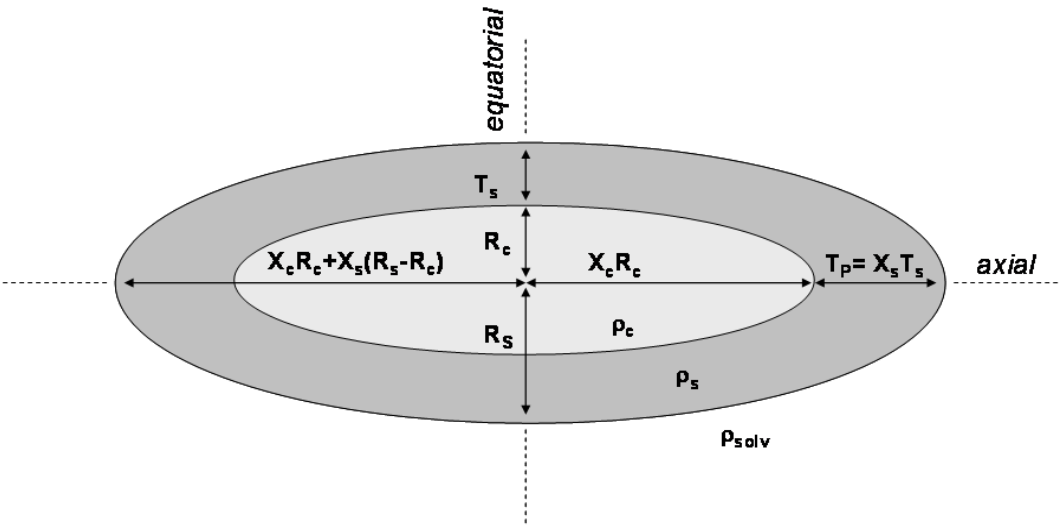

Figure 2 – Core-shell prolate ellipsoid of revolution model chosen to fit the SAXS data

For a constant shell thickness, X_S= 1, the fit gives a $\chi^2/Npts$ value around 13. However, the best fit ($\chi^2/Npts$ = 6.7) is obtained for a slightly negative X_S value (X_S ~ -0.2) corresponding to a small and negative polar shell thickness in the axial direction, T_P, of the core-shell ellipsoid of revolution model.

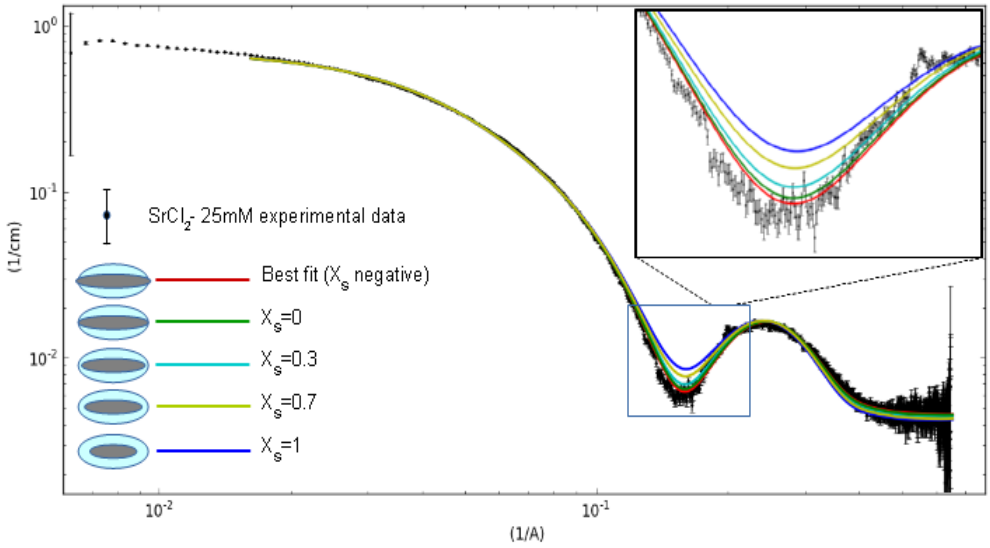

Figure 3: SAXS curve recorded on the $SrCl_2$-25mM system: influence of X_S (polar shell ratio) value on the calculated curves obtained with a core-shell ellipsoid of revolution form factor. Best fit is given in red.

In Figure 3, we report a typical SAXS curve recorded on sample 7 ($SrCl_2$-25mM), which shows a series of fits using the same core-shell prolate ellipsoid of revolution form factor model and a variable X_S, allowed to vary between 0 and 1. It can be clearly seen that the bottom of the first minimum is best fitted with a negative X_S value, a fact which has no clear

physical meaning, as it supposes that there is a small part of the hydrocarbon core which is in close contact with the aqueous solvent at the end-tips of the ellipsoid in the axial direction. However, as the best fit is always obtained for $X_S < 0$, we impose $X_S = 0$ for all samples' profiles. We interpret this assumption as follows: the end-tips in the axial direction of the sophorolipid aggregates are somewhat difficult to describe and may consist of a quite disorganized assembly, containing COOH groups, sophorose, salt, water and part of the aliphatic chain.

It is important to note that whatever the absolute value of X_S, the trends obtained for the other variables is unchanged, as it can be seen from the comparison between the fit parameters for $X_S = 0$ presented in Table 3 (discussed later in more detail) and the fit parameters obtained for $X_S = 0.3$, shown in Table S2/Table S3 in the Supporting Information. Except the surprising feature of $X_S = 0$, all other variable parameters give realistic values: the equatorial core radius and shell thickness are around 7.7 and 12.3 Å respectively, and the shell SLD is 1.1 x 10^{-5} $Å^{-2}$ (387 e^-/nm^3), corresponding roughly to 73 % v/v of water in a simple water-sophorose composition of the shell (Table 4). The X_C ratio of 9.4 characterizing the elongation of the ellipsoid is slightly high, if it compared with previous results[33] and will be discussed thereafter.

The resulting shape that best describes the sophorolipid micelles is very close to a "coffee bean" like, with a variable shell thickness from T_S to 0, which is quite atypical with respect to the majority of both ionic, non-ionic and bolaform[16] surfactant systems, generally described by core-shell form factors with a homogeneous shell thickness.[19-21] Nevertheless, this peculiar shape is the best suited to fit at best all systems described in this work and a large number of complementary other systems.

All SAXS measurements were made at the same sophorolipid concentration, 80 mM, and at concentrations of salt and/or base in the range from 5 to 100 mM. Table 3 shows the model parameters (N_{agg}, R_c, X_c, z, ρ_s) for core-shell ellipsoidal micelles of the sophorolipids with either salt or a base at various concentrations, but also the calculated shell thickness (T_S) and volume fraction of CH_2 in the dry core (α). Table 4 presents the volume fraction of water ($x_{v,w}$), and number of water molecules per sophorolipid ($n_{w/SL}$) in the shell; these have been indicated for three possible headgroup (*hg*) scenarios: *hg_1* considers only sophorose and COOH (or COO^-); *hg_2* includes the *hg_1* hypothesis and the C_{17} and C_{18} atoms; *hg_3* considers the *hg_2* scenario as well as the contribution of CH_2 groups from the aliphatic chain

excluded from the core (13(1-α), where α has been defined in Eq.4 and experimental values given in Table 3).

First of all, the results show that the equatorial core radius R_C, which corresponds to the dry part of the micelle, is relatively small, between 6.0 and 8.0 Å, a value which is the lower limit of what is acceptable for the model. In return, the thickness of the shell, between 11.0 and 12.5 Å, is quite large if this value is compared with those reported in the literature for similar systems studied by SANS (~8 Å, ~3 Å), [33,36] a discrepancy that may be explained by the different contrasts inherent in each technique. At the same time, the value of α is contained in the range between 0.52 and 0.72 depending on the system and it mainly indicates that a significant proportion of the hydrocarbon chain is in an aqueous environment and that is the counterpart of the small core and large shell of these aggregates. This is expected for a bolaamphiphile, as quantitatively demonstrated here below.

Table 3 – Fit parameters obtained from the core-shell ellipsoid of revolution form factor using X_s= 0 (defined in Figure 2). N_{agg}= aggregation number; R_C= equatorial core radius; X_C= axial core ratio; T_S= equatorial shell thickness; ρ_s= scattering length density of the shell; α= fraction of CH_2 inserted in the dry core of the micelle (Eq. 4); z= charge per micelle.

Sample	N_{Agg}	R_C (Å)	X_C	T_S (Å)	ρ_S x 10^{-5} (Å^{-2})	α	z
RbCl-10mM	55	8.0	6.5	12.0	1.0741	0.70	
RbCl-50mM	64	8.0	7.7	11.7	1.0768	0.72	
RbCl-100mM	69	7.9	8.1	11.5	1.0829	0.69	
$SrCl_2$-5mM	52	7.7	6.9	12.4	1.0608	0.71	
$SrCl_2$-25mM	72	7.7	9.4	12.3	1.0611	0.72	
$SrCl_2$-50mM	73	7.8	8.9	11.8	1.0751	0.69	
RbOH-40mM	34	6.6	5.5	12.3	1.0618	0.55	6.8
RbOH-80mM	24	6.1	4.7	11.0	1.0707	0.53	9.9
$Sr(OH)_2$-10mM	50	7.2	6.8	12.6	1.0632	0.59	4.6
$Sr(OH)_2$-20mM	41	7.0	5.4	12.3	1.0785	0.52	5.0

Table 4 - $x_{v,w}$= volume fraction of water in the shell (Eq. 7) and $n_{w/SL}$= number of water molecules per sophorolipid (Eq. 8). Several compositions of the headgroup are considered: headgroup 1, *hg_1*≡ sophorose + COOH; headgroup 2, *hg_2*≡ sophorose + COOH + CH (C_{17}) + CH_3 (C_{18}); headgroup 3, *hg_3*≡ sophorose + COOH + CH (C_{17}) + CH_3 (C_{18}) + 13(1-α)CH_2. Grey-shaded area refers to the hypothesis best describing the shell composition.

Sample	$x_{v,w}$			$n_{w/SL}$		
	hg_1	hg_2	hg_3	hg_1	hg_2	hg_3
RbCl-10mM	0.70	0.65	0.54	32	29	23
RbCl-50mM	0.69	0.64	0.54	31	28	22
RbCl-100mM	0.68	0.63	0.51	29	26	20
$SrCl_2$-5mM	0.73	0.68	0.59	37	34	28
$SrCl_2$-25mM	0.73	0.68	0.59	37	34	28
$SrCl_2$-50mM	0.70	0.65	0.54	32	29	22
RbOH-40mM	0.73	0.68	0.53	37	34	24
RbOH-80mM	0.71	0.66	0.49	33	30	21
$Sr(OH)_2$-10mM	0.72	0.68	0.54	36	33	24
$Sr(OH)_2$-20mM	0.69	0.64	0.46	31	28	18

Shell hydration vs. ion condensation

$n_{w/SL}$ gives an estimate of the number of water molecules per sophorolipid in the shell. As shown in Table 4, this parameter strongly depends on the supposed composition of the dry headgroup. If one only considers the sophorose and COOH groups to be part of the shell (*hg_1* hypothesis in Table 4), $n_{w/SL}$ varies between 29 and 37. In the hg_2 scenario (*hg_1* plus CH and CH_3), $n_{w/SL}$ does not vary much, as it is comprised between 26 and 34, indicating that inclusion of CH and CH_3 in the headgroup does not have a substantial impact on the shell hydration. Finally, if one includes the fraction of CH_2 not included in the core ($13(1-\alpha)$), *hg_3* hypothesis in Table 4, the hydration is sensibly lower and $n_{w/SL}$ now varies between 18 and 28. As first comment, we must state that these estimations should be taken with caution, because our SAXS model does not include the presence of ions in the shell, which can also be responsible for the variation of the shell SLD. The proportion of ions in the shell could be controlled in the fit through, for example, an adjustable parameter k= number of cations per sophorolipid in the shell. However, k cannot be determined without fixing the number of water molecules per sophorolipid, both parameters influencing the value of ρ_S in opposite ways: ionic species increase the value of ρ_S, whereas water molecules decrease it. By neglecting the influence of ion concentration, the number of water molecules per sophorolipid is adjusted to account for both effects, so that an increase of ρ_S leads to a decrease of $n_{w/SL}$ even if it can come in reality from an increase of the ion condensation. As a result, the number

of water molecules per sophorolipid reported in this case can be interpreted as minimum values, even if the space filling requirement may also have an influence. This approximation will be confirmed by the ASAXS experiments, which will show that the amount of counterions in the shell is practically negligible, unless their concentration becomes important.

Secondly, values of $n_{w/SL}$ above ~25 are higher than expected from the literature about glycolipids and disaccharides. It is well-known that hydration properties of disaccharides with the same chemical formula as sophorose (maltose, sucrose and trehalose, $C_{12}H_{22}O_{11}$) but different structures, are different, depending on the solute-water interactions.[81,82] Effects coming from the linkage type between the two glucose unit (sophorose is a glucose β(1,2) saccharide), the position of hydroxyl groups, the number of intracellular hydrogen bonds may influence the hydration properties of disaccharides and have been extensively studied. For example, the headgroup hydration number of maltoside surfactants is reported to be 8 in the case of SAXS studies[83] and in Abel *et al.*[84] with MD simulations. For the trehalose, which is known as being slightly more hydrated than maltose,[81,82] Lupi *et al.*[85] report values taken from literature that lie between 4 and 18. It is well-known that hydration numbers reported depend on the experimental method and/or assumption adopted. Ultrasonic measurements give values among the highest, and MD simulations for which the hydration number is defined as the number of H-bound water leads to similar values (around 15 to 18) suggesting that these experimental hydration numbers mainly refer to water molecules directly involved in H-bonds with the solute. In contrast, in their study on hydration and mobility of trehalose in aqueous solution, Revsbech Winther *et al.*[86] used a geometric hydration number, identified as the number of water molecules required to cover the solute with one layer (47 water molecules per trehalose).

The values obtained in this work are for a micellar shell composed of a sophorose group, that is a disaccharide and the hydration properties of which, if they are reasonably expected to differ from maltose and trehalose, should still not be excessively high. For this reason, the *hg_3* hypothesis provided in Table 4 is most likely to be real, as reasonable values are certainly the ones including the COO^- (or COOH), the CH and CH_3 groups but also 13(1-α)CH_2 groups and an unknown, and variable, number of ions, depending on the sample composition. More than reasonable, *hg_3* hypothesis is actually expected: if hydration numbers of COOH, CH_2 and CH_3 are reported to be small, 1.153, 0.999 and 0.586 respectively,[87] it is expected the aliphatic chain portion close to the headgroup to be hydrated. Typical estimations (both experimental and theoretical) for alkylammonium salt and SDS

surfactants are that up to 3 CH_2 groups from the polar head can be hydrated.[50-52] In this work, we find between 4 and 7 hydrated CH_2 groups per sophorolipid (calculated as $13(1-\alpha)CH_2$, where α is given in Table 3); these values can reasonably be expected for a system containing two polar headgroups. On the other hand, hydration number of ions is higher and, depending on the ionic concentration, it can influence the SLD of the shell quite heavily: reported hydration numbers lie between 6 and 8 for Rb^+, between 4 and 8 for Na^+,[88] and between 7.3 to 10.3 for Sr^{2+}.[89] According to the ASAXS experiments reported in the next section and showing a negligible amount of counterions in the shell, one can consider the amount of hydration water to be also negligible.

If the contribution to the hydration from all species can reasonably explain the experimental values of $n_{w/SL}$ found here, one should still take these values with caution, given the wide range of variation of the theoretical values. Moreover, there is no indication that the micelle shell does not contain free water that is not accounted for in the hydration numbers reported. The shell hydration may also be strongly related to the conformation of sophorolipids within the micelle, depending on the molecular structure of the sophorolipid and its impacts on the micellar structure.

As we can see from Table 3, the shell thicknesses reported here are always greater than 10.5 Å and usually between 11.0 and 12.5 Å, a range of values which seems to be high compared to the size of the sophorose alone, estimated to be below 10 Å,[32] 7.3 Å in poly-sophorolipids,[90] or 9 Å for trehalose.[86] The shell thickness of SL micelles determined by SANS was also reported to be around 8 Å.[33] The quite thick shell found here may take into account the "roughness"[4], confirmed by the MD simulation in the next sections, of the apolar core and hydrated shell interface coming from the presence of CH_2 in the hydrated shell environment. We can estimate the typical separation distance between sophorose molecules in the shell from the sophorose molar concentration (0.93-1.34 $mol.L^{-1}$.) to be around 3.5-5.1 Å, by using molecular parameters of trehalose (see Ref 86). This space, filled by the other components of the shell, can accommodate one water layer, and even if there are some alkyl groups in close contact with the sophorose, regarding the geometric hydration number of 47 for trehalose in water, the number of water molecules per sophorolipid in the shell presented here, which lie from 20 to 30, in the hg_3 hypothesis, does not seem outrageous.

Table 5: Area parameters; $A_{mic,w/SL}$ = area per sophorolipid at the micelle/solvent interface; $A_{C,S/SL}$ = dry core/hydrated shell interface; $A_{alkyl/sopho}$ = area per sophorolipid between the alkyl chain and the sugar/carboxylate headgroup; L = average length between the headgroups

Sample	$A_{C,S/SL}$ (Å)	$A_{alkyl/sopho}$ (Å)	$A_{mic,w/SL}$ (Å)	L (Å)
RbCl-10mM	75	104	196	3.76
RbCl-50mM	76	103	194	3.69
RbCl-100mM	74	102	187	3.49
$SrCl_2$-5mM	78	108	213	4.21
$SrCl_2$-25mM	79	106	208	4.19
$SrCl_2$-50mM	75	103	193	3.72
RbOH-40mM	71	124	219	4.04
RbOH-80mM	75	141	231	3.72
$Sr(OH)_2$-10mM	70	111	204	4.03
$Sr(OH)_2$-20mM	64	112	190	3.48

Area per sophorolipid

Another interesting piece of information is given by the analysis of the area per sophorolipid at the micelle/solvent interface ($A_{mic,w/SL}$), and at the dry core/hydrated shell interface ($A_{C,S/SL}$, see Table 5). These are calculated using the classical formula for the surface area of a prolate ellipsoid divided by N_{agg}; the values of the semi-axes, as defined in Figure 2, are given in Table 3. Micellar structure of dodecyl maltoside has been described by Cecutti *et al.*[91] showing that ellipticity of the micelle comes from the bulky hydrated maltose headgroups and their perpendicular conformation to the interface. Area per dodecyl maltoside at the micelle/solvent interface and at hydrophobic core/sugar headgroup interface are 87 and 50 Å^2, respectively. In the case of sophorolipids, however, one must keep in mind that there is one alkyl chain and two different polar heads per surfactant, leading to values lying from 187 to 230 Å^2 per sophorolipid at the micelle/water interface, and from 64 to 79 Å^2 per SL at the core/shell interface, depending on the sample composition. Another point to consider is that the core/shell interface in our case is located quite far from the sugar headgroup, considering the α value lying around 0.52 - 0.72. If the alkyl chains are perpendicular to the core/shell interface, we can estimate the area per sophorolipid between the alkyl chain and the sugar/carboxylate headgroup $A_{alkyl/sopho}$ to be the surface per SL of an ellipsoid of equatorial radius R_C+6.5(1-α)1.265 and axial radius $R_C X_C$+6.5(1-α)1.265 (noticing that this surface may be slightly overestimated as the influence of the X_S parameter is neglected). In this case, areas reported lie between 102 to 141 Å^2 for the most ionized micelles, comparable to that reported by Chen *et al.*[92] for SL at air-water interface (104 Å^2).

Ionic and basic effects

According to the results in Table 3, some general observations can be made regarding the effect of salts on sophorolipids micelles. First, the salts cause an elongation of the micellar aggregates and subsequent increase of the aggregation number, while the diameter of the core remains constant. For instance, increasing RbCl from 10 mM to 100 mM, it produces an increase of X_C from 6.5 to 8.1, whereas R_C is practically 8 Å. However, it appears that the elongation due to the presence of salt has a limit, observed through N_{agg} and X_C values which increase rapidly between 10 and 50 mM of RbCl (5 and 25 mM of $SrCl_2$) and then seem to reach a plateau at higher concentration, around 73 for N_{agg} and 8.5 – 9.0 for X_C. Another fairly clear effect of adding salt is the slight shell shrinkage and the concomitant dehydration observed through the shell thickness (T_S), the volume fraction of water in the shell ($x_{v,w}$) and the decreasing number of water molecules per sophorolipid ($n_{w/SL}$).

The shell SLD, ρ_S, is in the range between 1.06 and 1.09 x 10^{-5} $Å^{-2}$, where the smaller value is systematically observed for the $SrCl_2$ salt system. Small differences between the two salts is also observed on the values of R_C, T_S, $x_{v,w}$ and $n_{w/SL}$. The sophorolipids micelles in the presence of $SrCl_2$ have slightly smaller cores, a shell slightly thicker and hydrated than in the presence of RbCl. These differences have no impact on the value of α that remains constant for all the salt systems, and quite high (around 0.69 - 0.72). The aggregation number N_{agg} is slightly smaller for $SrCl_2$ at low salt concentration (52 vs 55), while at higher concentration the elongation of sophorolipids micelles is more pronounced with $SrCl_2$ than with RbCl (X_C reached a value of 8.9 for $SrCl_2$ and 8.1 only for RbCl). Areas per sophorolipid and the average length between the headgroups, L, reflect these small differences, being slightly higher for $SrCl_2$ than for RbCl (Table 5).

Adding a base to sophorolipids micelles solutions considerably changes the physico-chemical parameters. First of all, one observes the appearance of intermicellar interactions, accounted here with the introduction of a structure factor described with a repulsive screened Coulombic intermicellar interaction potential. This is consistent with what it was previously reported.[33] In terms of micellar size, the equatorial core radius is dramatically reduced, from 7.2 Å for the less basic system ($Sr(OH)_2$ – 10 mM) to 6.1 Å for the most basic system (80 mM RbOH) while the X_C ratio is much smaller than those reported above, decreasing to values smaller than 6 for all [OH^-] higher than 40 mM. The aggregation number follows this trend, decreasing to 24 for RbOH 80 mM. α also undergoes a fall, reaching values around

0.52, which indicates that in basic medium, half of the total amount of CH_2 are located in an aqueous environment. These trends are consistent with an increase of the micelle curvature due to the increased electrostatic repulsion taking place between more ionized headgroups. The shell thickness is practically invariable (12.3 Å) for the less basic samples (RbOH-40 mM and $Sr(OH)_2$-20 mM) and substantially decreases (11.0 Å) at high concentration of RbOH. Finally, Figure 4 shows the typical SAXS profiles of sophorolipids in the presence of $SrCl_2$ and $Sr(OH)_2$, showing the experimentally found spectral differences and a pictorial imaging of the salt and base effect on the micellar size.

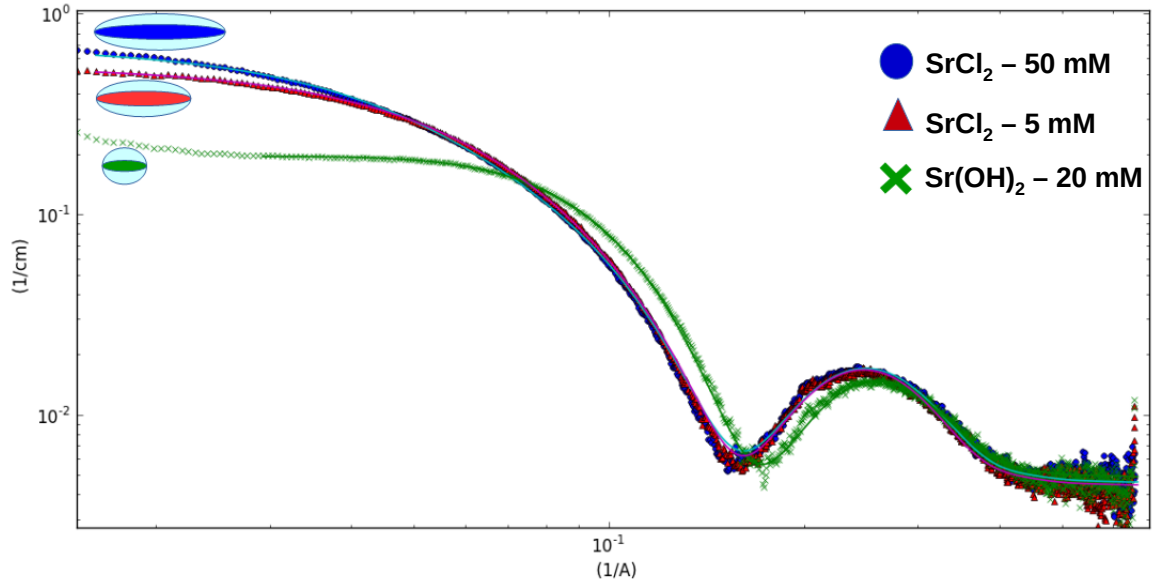

Figure 4 – SAXS spectra of sophorolipids in the presence of $SrCl_2$ and $Sr(OH)_2$. The pictures represent the ellipsoidal nature of the micelle with a X_s= 0, as commented before. The difference in longitudinal dimension among the ellipsoids is based on the data obtained from the best fits and presented in Table 3

Counterion distribution in the salt systems studied by ASAXS

ASAXS is a powerful method to put in evidence the distribution of counterions in soft matter, and in particular around polyelectrolytes and micelles.[57-62] It was employed to describe the charge distribution around charged polymers,[58,61] DNA and RNA[93] and CTAB micelles. [60,62] In this study, ASAXS is employed with the goal of revealing indirectly the distribution of the COO^- groups, if one assumes that its negative charge is neutralized by a counterion upon increasing the solution pH. In this case, the SAXS spectrum shows a broad scattering hump, which can be nicely fitted using a Screened Coulomb potential, as it was previously done in SANS experiments.[33] The resulting negative charge of the micelles settles between -5 and -10 (Table 3) and it clearly increases upon increasing the amount of base for

both Rb^{+} and Sr^{2+}. ASAXS can be used both in a qualitative and quantitative way.[62,63] If the former tells about the space distribution of counterions, the latter provides data on the amount of counterion in the proximity of charged macroions and even their binding degree. However, the quantification process can be very delicate[60,61,94] and it was mainly used so far on either polyelectrolytes or robust micellar systems.

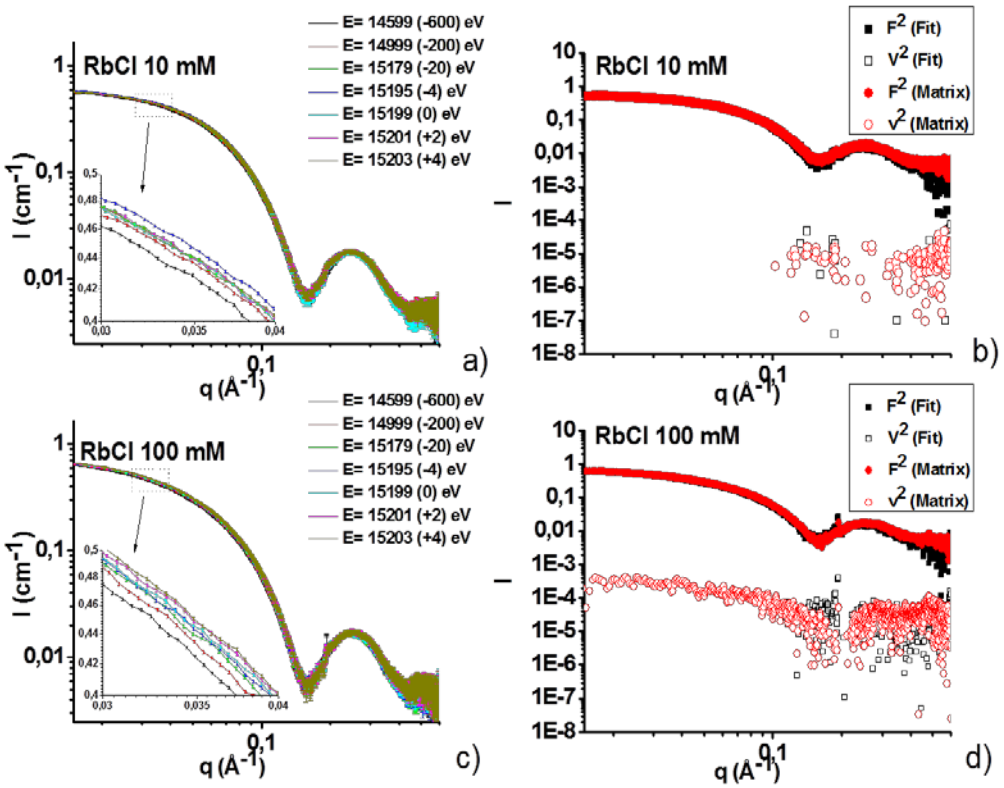

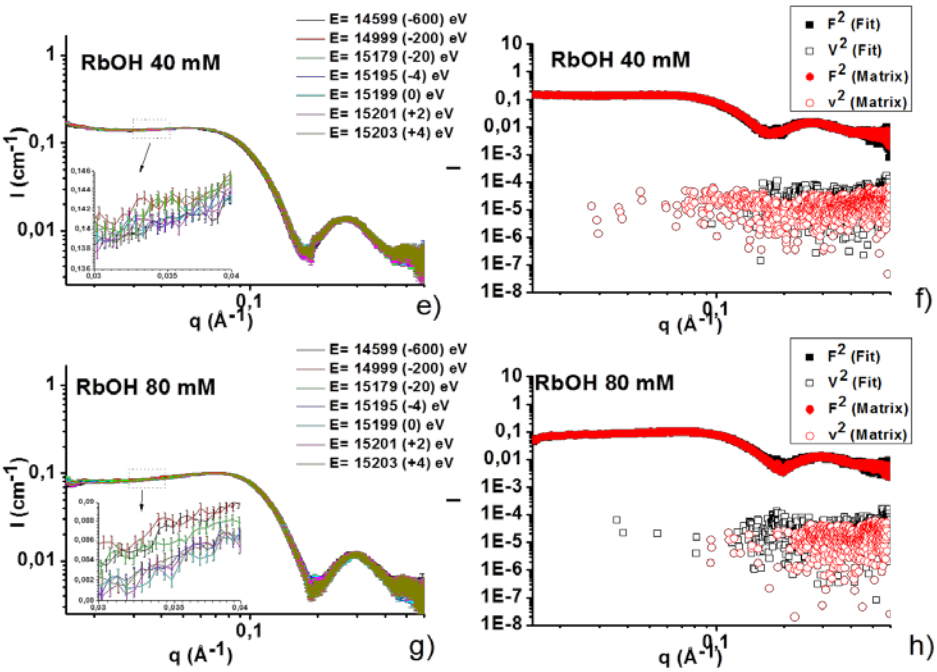

Figure 5 – a, c, e, g) Energy-dependent SAXS spectra for the sophorolipid - RbCl (10, 100 mM) and RbOH (40, 80 mM) systems. The energies at which the spectra have been recorded are indicated in the figure. b, d, f, h) $F^2(q)$ and $v^2(q)$ scattering profile of the cation (Rb^+ and Sr^{2+}) as obtained from the ASAXS treatment of the spectra. More experimental details are presented on Page S6 in the Supporting Information.

Figure 5 shows the typical scattering profile, *I(q)*, recorded for the RbCl (10, 100 mM) and RbOH (40, 80 mM) systems at the incident energy E= 14599, 14999, 15179, 15195, 15199, 15201, 15203 eV, corresponding to the ΔE_{Rb+}= -600, -200, -20, -4, 0, +2, +4 eV (treatment of background is shown in Figure S2 in the Supporting Information). The ASAXS results are only shown for the RbCl system but very similar conclusions can be drawn for the $SrCl_2$-containing samples, and for this reason they will not be reported here. As explained in the experimental section, fluorescence contribution has been subtracted for all spectra. At a first glance, spectra are very close to each other but a closer look in the inset of Figure 5a,c, for instance, indicate that *I(q)* appreciably (with respect to the error bars) increases with increasing energy (colour sequence: black, red, green, blue...) for both the RbCl 10 mM and 100 mM systems. This effect is expected in the case of an anomalous effect upon varying energy through the edge and it demonstrates that Rb ions decorate the micellar outer surface. Nevertheless, variation in *I(q,E)* is very mild; at 100 mM RbCl (Figure 5c), a concentration in counterions at which the anomalous effect was reported to be very important for polyelectrolytes and ionic surfactants systems,[62,63] *I(q,E)* only varies by a factor 1.04 when

measured far below and at the absorption edge [I(0.03,14599)= 0.47 cm^{-1} compared to I(0.03,15199)= 0.49 cm^{-1} at the Rb^+ edge], while expected variations should not be less than a factor 2. This is further demonstrated by the splitting of *I(q)* into the $F_0^2(q)$ and $v^2(q)$ components, respectively, the nonresonant intensity of the macro-ion and the pure resonant contribution of the counterion, shown in Figure 5b,d. The splitting shows no noticeable effect on the 10 mM system using both the matrix and fit methods, and a mild anomalous effect on the 100 mM system, but only employing the matrix method. This last result is coherent with the higher salt amount present in this system, thus indicating that part of Rb^+ cation in solution decorate the micellar shell. This result helps better understanding the evolution of the shell SLD (ρ_s) commented in the SAXS section (Table 3). One can now affirm that the amount of salt in the shell is below the limit of detection of the ASAXS technique, which can reasonably be settled in the mM range. This shows that the very small increase in the ρ_s, found for the RbCl, but also the $SrCl_2$ systems, is most likely due to a true variation in the number of water molecules per sophorolipid. However, for the higher RbCl concentrations (e.g., 100 mM), one cannot exclude the presence of larger amounts of salt in the shell, a fact which may also, as commented before, account for the mild increase in ρ_s. Interestingly, in the presence of salt alone, the equilibrium pH of a sophorolipid solution is slightly below 5. The corresponding experimental ionization degree ($\frac{[COO^-]}{[COOH]+[COO^-]}$), calculated from the titration curve (Figure S3 in the Supporting Information), is below 5 %. This means that at high salt content, counterions decorate the hydrophilic shell independently from the presence of carboxylate groups. In terms of quantification, the mild anomalous effect recorded does not allow a reasonable quantification of the amount of counterions-per-sophorolipid.

Upon addition of RbOH, carboxylic groups deprotonate into carboxylates, which carry their respective counterions, our hypothesis[33] being that the negative charges are settled at the micellar/water palisade. Under these assumptions, this effect should be detectable by ASAXS at a larger extent with respect to the base-free medium. The corresponding experiments in Figure 5e,g show, on the contrary, that *I(q)* undergoes no sensible evolution with the incident energy, as all curves practically lie with in a small range comprised in the error bars. The poor anomalous scattering effect is confirmed by the signal splitting using both the fit and matrix methods (Figure 5f,h), which do not provide a significant $v^2(q)$ component. Since similar results are obtained with $Sr(OH)_2$, these will not commented further. How to interpret this result? One of the main results so far is the fact that the bolaform morphology of

sophorolipids promotes the formation of "non-standard" micelles. By this we intend a micelle that does not have a homogeneous hydrophobic core well-separated from the hydrophilic corona with constant thickness. The size of micelles and the aggregation number sensibly decrease upon addition of a base (Table 3) and a partial solubilisation of sophorolipids in solution should not be excluded. Such a scenario could suggest that not all COO^- groups do actually settle in a narrow region at the micellar/water interface, but they could be randomly distributed in the thick shell region, being closer to the hydrophobic core. If resonant species (the counterions) penetrate deeper inside the micelle, the difference in terms of core-shell SLD at the element absorption edge will be attenuated, and one expects the ASAXS signal to be attenuated. This scenario could be suggested by the larger number of hydrated CH_2 (about 6 per sophorolipid, for an α parameter close to 0.5, Table 3) and not excluded with respect to old works on ionic/neutral bolaamphiphiles[22,23] and according to which water can penetrate deep inside a bola's micelle. However, a comparison with previous ASAXS studies is difficult because all of them have been carried out on either polyelectrolytes or micellar surfactant systems with a well-defined core-(charged)shell interface (e.g., CTAB). In both cases, there are no doubts about the localization of the counterions. Even if fluctuations in the counterion distribution is probably amplified in the case of sophorolipids due to a redistribution of the carboxylate groups away from the outer micellar layer, this phenomenon has been already reported to potentially affect ASAXS measurements on other systems. In micellar systems (TTAB), fluctuation of the counterion cloud was shown to affect the scattering intensity of the macroion (TTA^+) at $q > 0.2$ Å^{-1}.[95] In a rod-like polyelectrolyte, it was shown that longitudinal fluctuations of the number density of the counterions affect SAXS data at $q > 0.3$ Å^{-1} and they can actually be measured experimentally.[59,61] Finally, fluctuations due to the polydispersity of the number of acrylic acid (PAA) chains on polystyrene (PS) was also shown to affect the pure resonant curve $v^2(q)$ at q> 0.04 Å^{-1}. According to these works, it seems possible that, if fluctuations of the COO^- distribution occurs in sophorolipid micelles upon addition of a base, the corresponding $v^2(q)$ profile will inevitably be affected. It seems that in all systems where the macroion (polyelectrolyte, micelle) charge density is well-defined and located at the surface, only the counterions number density fluctuations at the macroion surface should be considered. In this case, the $v^2(q)$ profiles will be affected at (relatively) large q values above 0.2 Å^{-1}, which, in the case of sophorolipid micelles, may not play an important role afterall. On the contrary, if fluctuations of the macroion charge distribution are experienced, as seen in the case of PAA-PS system, the affected q-range may be much larger, starting at $q < 0.1$ Å^{-1}. In this specific case, the effect on the $v^2(q)$ profile for sophorolipid micelles may not be

negligible. We then expect that if the COO^- distribution will occur at the micellar surface only, the $v^2(q)$ will be enhanced, while if the COO^- distribution will occur in the interior of the micelle, the $v^2(q)$ will be reduced. We believe that the second scenario does occur in the sophorolipid-based system upon addition of a base.

Contrast matching by Small Angle Neutron Scattering

In the SAXS section, we have shown that sophorolipid micelles at 80 mM adopt a non-conventional "coffee bean" like structure, the length of which is slightly influenced by the amount of salt or base. By "coffee bean" like structure we have intended the fact that the composition at the extremities in the axial direction of the micelle is hard to describe with a simple core-shell model and they are most-likely constituted by a mixture of aliphatic chain, sophorose and COOH groups. According to the ASAXS experiments, we could also put in evidence that the distribution of the COO^- groups is not only confined at the micellar surface but it is probably random in the thick hydrophilic region. Unravelling the distribution of the sophorolipid molecule inside a micelle can be approached through a direct experiment which consists of "visualizing" the distribution of the oleic acid, or the sophorose group by mean of contrast variation SANS. This experiment consists into matching the SLD of a given section of a particle, or molecule, via a well-chosen mixture of deuterated and hydrogenated solvent, the SLD of which can be tuned by playing on the relative ratio between the two. In the case of SL micelles, it is possible to look at the scattering of the oleic acid, or sophorose, alone by choosing the correct proportion of D_2O and H_2O. Sophorose headgroups can be matched with a 46% D_2O, while oleic acid can be matched with 8% D_2O. Here, we prefer the first approach because experiments with large amounts of H_2O will suffer from the strong incoherent diffusion of hydrogen, inherent to the technique, and which are responsible for a critical increase in the background level. A complete match between the solvent and sophorose will give an idea of the spatial distribution of the pure aliphatic-containing core.

Figure 6 shows the typical SANS curve of a salt-free 80 mM solution of acidic SL in pure D_2O, the description of which is given elsewhere[33] and the geometry of which we now assume to be "coffee bean" like, as largely commented above. Without going into a further model-based analysis, we simply display the corresponding Indirect Fourier Transformation method (IFT), from which it is possible to evaluate the shape of an aggregate from the corresponding Pair Distribution function, *P(r)*.[96] The *P(r)* of a 80 mM solution of SL in D_2O (Figure 6b) of course reflects the I(q) data and it is typical for highly elongated object, in agreement with the SAXS data presented above and previous data recorded on a similar

system.[32] If the hypothesis of a homogeneous core-shell ellipsoid (the shell being of constant thickness and homogeneously composed of sophorose and water only) is correct, then one should expect, after matching the contrast between sophorose and the solvent, a SANS profile describing an ellipsoidal micelle being smaller in size (only the core will contribute). The SANS scattering profile of the contrast-matched (46% D_2O) SL solution is shown in Figure 6a (blue circles) and it presents two interesting features. First of all, the low-q intensity is decreased by a factor 100 with respect to the fully deuterated medium; this is a direct proof that the experiment was successful. In fact, according to Eq. 1, the intensity is directly proportional to the contrast between the object and the solvent. By matching the SLD between the sophorose and the solvent, the contrast only occurs between the core and the solvent and it is thus reduced, thus contributing to decrease the scattered intensity. The second point concerns the micellar shape and size after contrast matching. The *P(r)* function at 46% D_2O (Figure 6b) is typical of a much less elongated morphology, closer to a spheroid, if compared to the fully deuterated system. This suggests that a pure aliphatic core is mainly concentrated in a spheroidal region located at the center of the micelle.

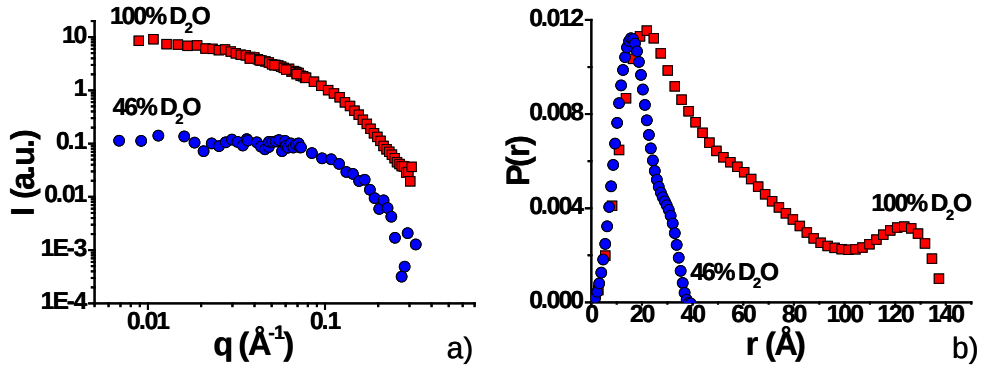

Figure 6 – a) SANS curves recorded on a 80 mM system of SL in 100/0 D_2O/H_2O (red squares) and 46/54 D_2O/H_2O (blue circles); b) Pair distribution function, *P(r)*, issued from data in a).

This experiment gives credit to, and it actually refines, the sophorolipid micelle model deduced from SAXS analysis. At the equilibrium pH (< 5) and at 80 mM, the sophorolipid micelle should be considered as a prolate ellipsoid divided into three regions, as identified in Figure 7: Region I is composed of a fully aliphatic core and the morphology of which is practically spherical; Region II constitutes the end-tips in the axial direction of the ellipsoid and it is a less defined region composed of aliphatic, sophorose and COOH groups. Region I is directly identified by contrast matching SANS experiments while region II is deduced by the fitting SAXS data using a “coffee bean” like model. Finally, Region III is identified as

being the outer shell composed of sophorose, COOH groups, water and, possibly, counterions. Contribution from vicinal CH_x groups should not be excluded, as detailed in the headgroup, *hg_3*, hypothesis of Table 4. As commented before, the contribution of salt plays a role on the ellipticity of the micelle, only but neither on its diameter nor its configuration. Furthermore, the ASAXS data show that the amount of salt in the sophorose surrounding is most likely negligible at least up to 100 mM. The orientation of the sophorolipid molecule within the micelle is sketched in Figure 7. Considering the typical micellar dimension with respect to the sophorolipid size, it seems highly probable that molecules can either cross the micelle from one end to the other, or bend in such a way that the COOH and sophorose groups belonging to the same molecule both lie in the same side of Region III. The addition of small amounts of base (pH range comprised between 5 and 7) promotes electrostatic repulsion among micelles induced by the deprotonation of the COOH into COO^-. According to the ASAXS data showing a non-existing anomalous effect in the presence of both Rb^+ and Sr^{2+}, we believe that in the intermicellar interaction regime, the negative COO^- groups and their respective counterions do not seem to be distributed only at the external micellar-water palisade, as we previously hypothesized,[32,33] but most likely to occupy the entire hydrophilic shell region.

Several authors have tried to study the structure of bolaform amphiphiles and in particular the one of glucose-containing units. The group of Vill has published several works on the micellar formation of bolaform glycolipids, mainly symmetric[18] and/or in mixture with anionic or glycolipid surfactants,[97,98] and they concluded that slightly ellipsoidal micelles could form, without going in detail in terms of the molecular distribution within the micelles. If similar works exist on other types of bolaform amphiphiles,[10,14] the precise description of molecular distribution is always a challenging task. Nagarajan,[21] basing his line of thought on geometrical considerations only, predicted in 1987 the self assembly behaviour of bola amphiphiles, mainly indicating the formation of spherical, cylindrical and vesicular objects. Interestingly, for spherical micelles he predicted a micellar radius equal to, or smaller, than half the full length of the hydrophobic chain. He also predicted interpenetration of the molecules and, for cylindrical micelles, local disorder at the end-tips in the axial direction of the cylinder. All these features, especially the disordered Region II shown in Figure 7, nicely confirm Nagarajan's models. Caponetti *et al.*[16] are the only ones who deeply discussed the distribution of *N*-azo-18-crown-6 ethers in micelles. Even if they did not provide a tentative image of their system, they discussed some interesting parameters. They used a core-shell ellipsoid of revolution form factor and used a homogeneous shell to fit their data. They found that between 15 and 20 water molecules are contained (bound and free) the hydrophilic

headgroup but none enters the core. They also found that addition of salt had no major effect on the core radius and shell thickness, even if some differences are found between LiCl and NaCl due to the respective difference in terms for complexation by the crown ether macrocycle. More insight on the structure of bolaamphiphile micelles, including molecular conformation, was also provided by Davey[19] and Shinde,[20] who worked on asymmetric bolaamphiphiles, alcohol derivatives of alkylammonium and oleate salts, that is ionic/neutral bolas analogous in structure to sophorolipids in the neutral pH regime. Interestingly, both authors agreed on the fact that micelles are spherical/ellipsoidal objects and on the fact both hydrophilic headgroups come in contact with the solvent at the micelle outer palisade, in contrast with older claimings according to which only the ionic headgroup is located at the micelle/solvent frontier while the non-ionic group is settled in the micelle interior, into which water easily penetrates. However, they do not agree on the molecular arrangements: Davey proposes an elongated cross-micellar conformation while Shinde proposes a bent configuration. If compared to the studies presented above, our more complex "coffee bean" like model presented in Figure 7 could be considered as a confluence of Nagarajan's[21], Davey's[19] and Shinde's[20] models together, in which the end-caps in the axial direction of the micelle are less defined and where the bolaamphiphile can adopt more than one configuration according to several parameters such as its position in the micelle itself, the aggregation number, the presence of salt, the ionic/neutral nature of one of the end-groups, the shell hydration state, etc… In order to verify the micellar model and sophorolipid distribution shown in Figure 7, we have used molecular dynamics simulations shown in the next section.

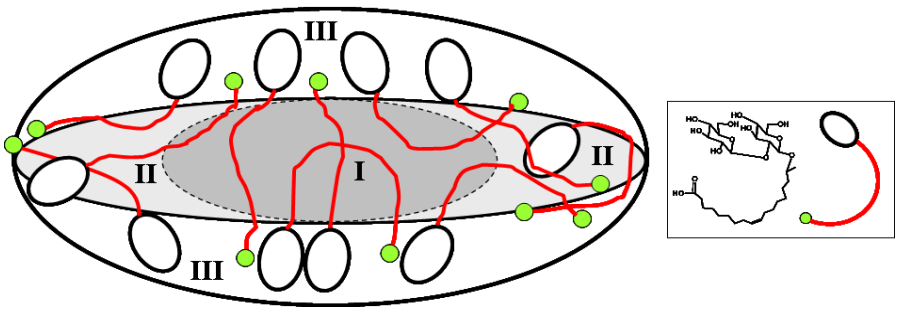

Figure 7 – Tentative model structure of an acidic sophorolpid micelle at its equilibrium pH (< 5). Region I= full aliphatic; Region II= mixed sophorose/water/COOH/aliphatic; Region III= sophorose/water/COOH. At 5 < pH < 7, the boundaries between the three regions are probably less defined and the COO^- groups occupy a broader volume in the hydrophilic region.

Molecular modelling by Molecular Dynamics.

In the following sections, we computed representative parameters (e.g. size, shape, surface properties, SL headgroup hydration and surfactant alkyl chain conformation) to characterize the micelle structure as a function of the SL aggregation number.

I. Aggregation process of the SL monomers into micelle. In Figure 8, we depict the SL aggregation process into a single aggregate for the MD2 simulation with 37 sophorolipids. The simulations results show that, in general, the aggregation process of the SL monomers into a single and stable micelle is relatively fast (~10 – 60 ns) and further analysis (not shown) also suggests that it occurs with two different time scales: one "fast" (t_{sim} < 10 ns) and one "slow" (t_{sim} = 10 – 60 ns) depending the system size as previously observed for others micellar systems (see, for instance, ref. 99 and references therein). For instance, in case of the MD2 simulation (Figure 8), it takes ~10 ns for that all SL monomers form small clusters with various sizes and shapes and ~55 ns for that the clusters form a single and stable aggregate. In the others systems, the aggregation time depends on the SL numbers and vary between 20 – 80 ns for the system with 27 and 68 SL, respectively. The stability of the aggregates can be also estimated by obtaining a constant radius of gyration, R_g, values of the aggregate (see next section) and agree with these values.

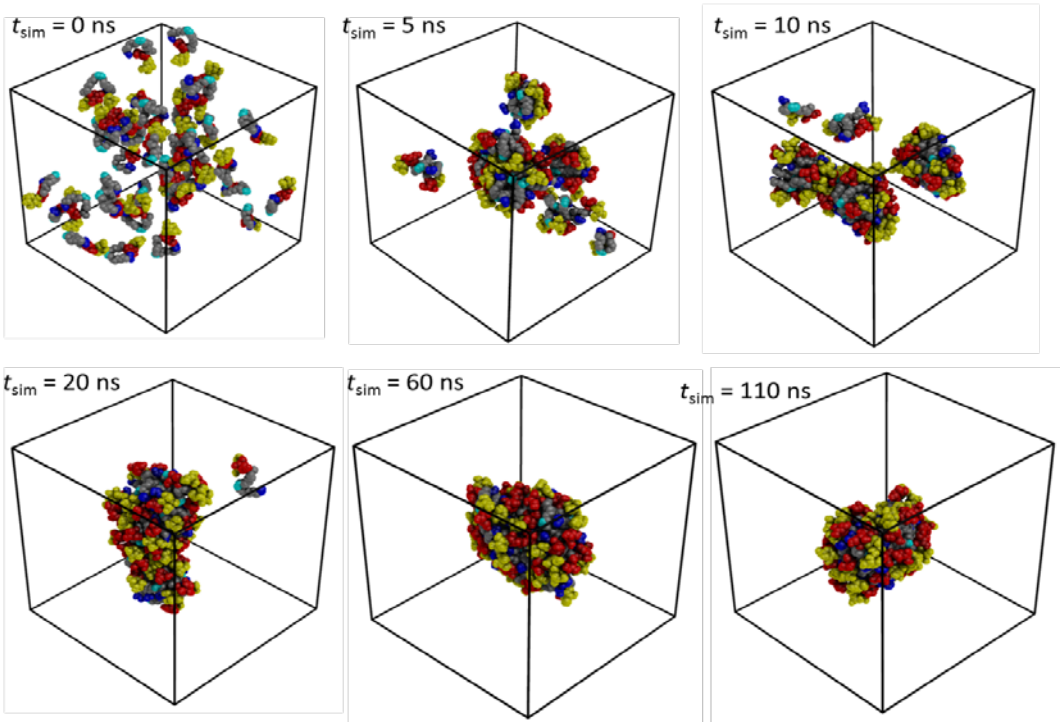

Figure 8 - Representative aggregation process of 37 SL monomers into a micelle *vs.* time for the MD2 run. The outermost and innermost glucose are colored in yellow and red, respectively, whereas the alkyl chain,

double bonds and COOH groups are in grey, cyan and blue colors, respectively. Water is not shown for visual clarity. The black line shows the box limits. The figures were drawn with PyMol.[100]

II. Micelle shapes and sizes

In Figure S4 in the Supplementary Information, we depicted the final structure of the aggregate as a function of the SL aggregation numbers obtained from the simulations. With the increase of the N_{agg} value, we observe a (quasi)sphere-to–(elongated) ellipsoid transition of the micelle shapes. At high N_{agg} value (i.e. MD6 system), the SL monomers form a structure to a spheroidal rod and this result does not depends on the SL concentration, since we found a similar shape with another simulation (not shown) where SL concentration was set 2 times lower. The micelle shape transition is actually in very good agreement with SANS data obtained on acidic sophorolipids in water as a function of concentration.[101]

To estimate more precisely the micelle shape changes during the course of the MD1-5 simulations, we employ a three-axis ellipsoid of revolution shape to model the micelles. The ellipsoid of mass M_T is identified by three semi-axis a_M, b_M and c_M ($a_M > b_M > c_M$) parameters, and the following equations[102]:

$$I_1 = \frac{1}{5} M_T (a_M^2 + b_M^2)$$
$$I_2 = \frac{1}{5} M_T (a_M^2 + c_M^2) \qquad \text{Eq. 19}$$
$$I_3 = \frac{1}{5} M_T (b_M^2 + c_M^2)$$

where I_1, I_2 and I_3 (with $I_1 > I_2 > I_3$) are the principal moments of inertia of the micelle. Please note that, with respect to the ellipsoid model in Figure 2 used to fit SAXS data, a_M is associated to the axial ($X_c R_c + T_P$) and b_M, c_M to the equatorial R_S dimensions.

The ratio between the major (a_M) and minor (c_M) semi-axis for the complete 28 – 80 SL micelle (a_M, b_M, c_M and $(a/c)_M$) are reported in the 6th column of Table 6. The computed micelle a_M, b_M and c_M values confirm that at low N_{agg} the micelle is nearly spherical and that the micelle change to a (pronounced) tri-axial ellipsoid with the increase of N_{agg}. At N_{agg} = 112 the aggregate form a rod shape oriented along the *y* axis and we may considered that the upper limit to have micelle is around 80 SL. Moreover, as noted previously[84] for similar micellar systems and in agreement with our experimental results, the shape of the micellar hydrophobic core is always significantly more ellipsoidal that the overall micelle ($(a/c)_{HC}$ and $(a/c)_M$ in range of 1.48 – 3.22 and 1.30 – 2.33, respectively).

By subtracting the semi-axis lengths of the aggregate hydrophobic core from those of the whole micelle, one can also obtain an estimation of the average thickness of the polar outer layer, l_{pl} (including the sophorose and the COOH groups, see last column of Table 6), which is nearly equivalent to the shell thickness (T_S) estimated from the SAXS data (Figure 2). We have to say that the estimation of the l_{pl} values from the semi-axis is quite rough and strongly depends on the presence of alkyl chain carbon atoms at the aggregate surface (and a_M, b_M and c_M values) that can underestimate in the l_{pl} calculations. The average polar layer thickness, l_{pl}, values change a little with the micelle shape and are in range of 4.9 – 5.1 Å for the aggregates with 28 - 80 SL monomers. In case of the aggregate with N_{agg} = 112, we estimate a l_{pl} value of 3.3 Å with only the b_M and c_M semi-axis. The computed l_{pl} values here are much smaller than the shell thickness values, T_S, obtained from the SAXS fit (>11.0 Å, see Table 3). l_{pl} value reflects the average shell thickness, which, according to SAXS data presented above, seems to be highly anisotropic, because T_S varies between ~11 Å (equatorial) and 0 Å (longitudinal), the average between these values, $<T_S>$, being in very good agreement with l_{pl}. The computed l_{pl} values, are consistent with those obtained previously for N-dodecyl-β-maltoside (DDM) micelles[84] where we found an average thickness for the α-maltose group (linear β(1→4) disaccharide) in range of 7.2 – 7.7 Å and consequently support the simulation results.

Table 6 - Aggregate size and shape. Values with M and HC subscripts were computed by including all the micelle atoms and those of the hydrophobic core, respectively. The radius of gyration, R_g^M, and the ellipsoid three semi-axis lengths (in Å) were computed from the inertia tensor (e.g., see ref. 102). a_M and c_M are the lengths and the radius of the rod. l_{pl} is the average polar layer thickness (including the sophorose and COOH groups) (in Å). The statistical errors (maximum errors) are always lower than 0.3, 0.5, and 0.2 Å for R_g, semi-axis lengths, and polar layer thickness, respectively. *In case of the MD6 system, due to its rod shape the $(a/c)_M$ and $(a/c)_{HC}$ values were not computed and the radius of gyration was obtained for a cylindrical rod of $2b_M$ length (equivalent to the box size) and an average radius of $(a_M+c_M)/2$.

System	R_g^M	a_M	b_M	c_M	$(a/c)_M$	a_{HC}	b_{HC}	c_{HC}	$(a/c)_{HC}$	l_{pl}
MD1	15.5	22.2	19.9	17.6	1.30	17.3	15.0	12.1	1.48	5.1
MD2	17.3	27.3	21.2	17.5	1.56	23.0	16.3	12.0	1.95	4.9
MD3	20.3	34.3	22.2	20.0	1.68	30.9	17.3	14.9	2.09	4.4
MD4	22.3	38.5	24.0	20.5	1.88	35.7	18.5	14.8	2.41	4.7
MD5	24.4	44.7	25.0	19.2	2.33	41.7	20.5	12.9	3.22	4.5

MD6*	23.4	14.7	40.2	12.2	-	11.1	-	10.1	-	3.3

To characterize the aggregate sizes, we computed the time evolution of R_g of the 5 micellar systems starting from the beginning of the production runs. As shown in the Figure S5, after large fluctuations of the R_g due to the SL monomers aggregation processes, the R_g values stabilize after 20 – 90 ns depending on the number of SL monomers in the box. We consider that all the SL monomers form a single and stable aggregate when the micelle R_g remain constant until the end of the simulation times. In the 2nd column of Table 6, we reported the average R_g for MD1-5 systems computed from the last 40 ns of each simulation. The values are found between 15.5 – 24.4 Å for the aggregates with 28 and 80, respectively. The values are in relative agreement with data found in this study (18 - 30 Å from the geometrical parameters detailed in Table 3 or computed from the Penfold values[36], and according to which the R_g (where $R_g^2 = \frac{1}{5}(a_M{}^2 + b_M{}^2 + c_M{}^2)$) for an ellipsoid of revolution, with a_M, b_M, c_M being the semi-axes of the ellipsoid obtained from the inertia tensor (see below). In case of the simulation with 112 SL, we obtained a $R_g \approx$ 23.4 Å from the expression for a cylindrical rod $R_g^2 = (\frac{R^2}{2} + \frac{L_{rod}^2}{12})$, where L_{rod} (here, $2b_M$) and R are average lengths of the rod and its radius (i.e. $(a_M+c_M)/2$ = 13.85 Å), respectively.

III. Aggregate surface contact properties and hydration

As shown in the MD snapshots depicted Figure S4, the surfactant different parts (i.e. sophorose headgroup and alkyl chain) are in contact with the solvent. To characterize more precisely the surface contacts shared between the aggregates and water, we computed the solvent accessible surface area (SASA) properties with two approaches. In the first one, we used the whole aggregate semi-axis lengths (a_M, b_M, and c_M) determined in the previous section and we calculated the SASA for an ellipsoid with a planar surface, $SASA_{SL}^e$, with the Knud Thomsen's Formula: $4\pi(\frac{a_M^p b_M^p + a_M^p c_M^p + b_M^p c_M^p}{3})^{\frac{1}{p}}$ where $p \approx$ 1.6075. Please note that this equation is valid for ellipsoids with three distinct semi-axes, so in case of the aggregate with 112 SL monomers that has a spherical rod shape, the $SASA_{SL}^e$ was estimated from the expression for an open cylinder (i.e. without the lateral areas): $2\pi RL_{rod}$, where R and L_{rod} are the characteristic dimensions of the rod defined just above. In the second approach, we

compute the SASA of the SL part in the aggregate (i.e. the headgroup, the double bond, the alkyl chain and COOH) by splitting the SL molecule into 6 parts (namely, the external and internal glucose ($SASA^V_{GLA}$ and $SASA^V_{GLB}$, respectively), the COOH group ($SASA^V_{COOH}$), the C7 alkyl chains separated by the C=C and bonded to the sophorose and COOH moieties ($SASA^V_{C7A}$ and $SASA^V_{C7B}$, respectively) and finally the two carbon atoms involved in the double bond ($SASA^V_{C=C}$). With these values, one can obtain the total SASA of each aggregate, $SASA^e_{SL}$ with $SASA^V_{GLA} + SASA^V_{GLB} + SASA^V_{COOH} + SASA^V_{C7A} + SASA^V_{C7B} + SASA^V_{C=C}$ = 100 %) (Table S5). These values were computed with the *trjVoronoi* program developed in our group (see ref. 99 and references cited therein). This program uses a Voronoi−Delauney tessellation[103,104] algorithm to estimate the surface shared between the SL and water atoms (excluding hydrogen).[105] In contrast to the first approach where we assume that aggregate is a planar tri-axial ellipsoid, in the latter calculation the micelle surface irregularity is fully taken into account. This is why the computed $SASA^V_{SL}$ values are always greater than $SASA^e_{SL}$ ones. By comparing the $SASA^V_{SL}$ and $SASA^e_{SL}$ values reported in Table S5 and by visual inspection of the simulation snapshots in Figure S4, one can deduce that the aggregate surface is quite rough, as also estimated by the analysis of the SAXS data above. To quantify this, we compute the surface rugosity factor ($f_{rug} = \frac{SASA^V_{SL}}{SASA^e_{SL}}$) and we found that f_{rug} values are always greater than 1.8 and slightly increase with SL aggregation number. For the aggregate with 112 SL monomers, we found a larger f_{rug} value (3.95) probably because we underestimate the $SASA^e_{SL}$ by considering the aggregate shape as a spherical rod. For sake of comparison, the computed f_{rug} values are found higher than those obtained in DDM micelles with similar size (1.6 – 2.0).[84]

From the $SASA^e_{SL}$ values, one can also estimate the area per sophorolipid at the micelle/solvent interface, A^e_{SL} with the expression $A^e_{SL} = \frac{SASA^e_{SL}}{n_{SL}}$. We obtained A^e_{SL} values lying from 177.4 to 132.5 Å^2 with SL monomers between 28 and 80 in fair agreement (discrepancy estimated between 10% and 30%) with the experimental estimation given in Table 5. In case of the aggregate with 112 SL monomers the A^e_{SL} is significantly lower (62.5 Å^2).

Concerning the $SASA_{SL}^{V}$ of each SL components, the values for the MD1-6 systems are reported in the 2nd – 7th columns of Table S5. The low SASA values for the alkyl chain and the double bond moieties (~14 and < 1 % of the total aggregate surface, respectively) indicate that these groups are protected from the solvent by SL headgroup or are buried in the hydrophobic core of the aggregates. For the sophorose and the COOH groups, they represent ~78 % and 8 - 9 % of the $SASA_{SL}^{V}$ values and tend to slightly decrease with the increase of the SL aggregation number are probably the consequence of the decrease of the micelle curvature and micelle shape changes leading to a different accessibility of the sophorose and COOH solvent to water.

To characterize the aggregate hydration, we have also computed the number of "unique" water (N_w) in the first shell (with a cutoff < 4.0 Å)[84] of whole aggregate, the sophorose, the COOH alkyl chain and double bond atoms (Table S6). The number of water molecules per sophorolipid is found to be ~27 for the smallest aggregate and it decreases to ~17 for the aggregate with 112. These results are in excellent agreement with the experimental data ($n_{w/SL}$), varying between 18 and 28 for the headgroup 3, *hg_3*, hypothesis, reported in Table 4. Moreover, the N_w values also confirm (as we noted from the corresponding $SASA_{SL}^{V}$ values), that the hydration of the sophorolipid is mainly due to the sophorose headgroup (as also found experimentally in the headgroup 1 hypothesis in Table 4) and at a less extent to COOH since these groups have 16.9 – 24.9 and 2.4 – 4.4 water in their first shells depending on the aggregate size. If small hydration values obtained for the alkyl chain and the C=C bond (3.1 – 5.0 and < 1, respectively), confirming the assumption made above about the accessibility of these groups to water, one should still observe that N_w for the alkyl chain varies between 3 and 5, which are very close estimates to what it is experimentally found in the *hg_3* hypothesis presented in Table 4. The slight decrease of the sophorose headgroup hydration as a function of the SL aggregation number may be caused by the slight change of the sophorose headgroup conformation and/or interaction between adjacent headgroup at the micelle surface.

To obtain a more precise picture of the SL headgroup hydration as a function of the SL aggregate sizes, we also computed the average number of nearest waters for each sophorose and COOH oxygen atoms (Figure 1) or $<n_{Ox\text{-}Ow}>$ from the computed radial pair density functions ($g(_{Ox\text{-}Ow})$) of the sophorose, and COOH (OC_{1A} and OC_{1B})-oxygen and water-oxygen (O_w) atoms (Figure S6). To obtain $<n_{Ox\text{-}Ow}>$ values, we integrated the RDF functions until the first minimum at r ≈ 3.5 Å after the first peak. No defined peaks at ~2.5 Å in the (O_{1A}, O_{1B},

O_{5A} and O_{5B}) RDFs indicate that these non-hydroxyl oxygen atoms are poorly hydrated by water in contrast to the sophorose OH oxygen. The computed $<n_{Ox\text{-}Ow}>$ values in Table S7 in the Supporting Information these observations. More specifically, the RDFs show that water molecules solvate primarily the hydroxyl oxygen (i.e. O_{2A}, O_{3A}, O_{4A}, O_{6A}, O_{3B}, O_{4B} and O_{6B}) of the sophorose headgroup and the COOH oxygen atoms (OC_{1A} and OC_{1B}). The only differences in RDFs between the different systems are for the amplitude of the first peak indicating variations of the number of hydration water molecules in the vicinity these oxygen atoms. The $<n_{Ox\text{-}Ow}>$ values for the sophorose hydroxyl oxygen atoms are close (1.8 – 2.4) between the six aggregates in contrast to the carboxyl ones where we observe a slight decrease of the $<n_{Ox\text{-}Ow}>$ values with the aggregate size (1.8 – 1.2 and 1.0 – 0.7). The hydrations of the ring oxygen (O_{5A} and O_{5B}) of the glucose are around 0.3 and 0.1, respectively. This is close to the value found previously[84] for the same atoms in maltose (~0.3 water). Finally concerning the oxygen atoms involved in the glycosidic bond (O_{1A}) and the link between the headgroup and alkyl chain (O_{1B}), the $<n_{Ox\text{-}Ow}>$ values (0.6) indicate these atoms are shielded from the solvent by the headgroup, as noted previously.[84]

IV. Conformation of the SL alkyl chain in the aggregates

Finally, we also examined the conformation of the sophorolipid as a function of the SL aggregation numbres by computing the distribution of the end-to-end distance between the first C1 and the C17 atoms, $P(d_{C1\text{-}C17})$, of the SL alkyl chain (Figure 1 and Figure S7 in the Supplementary Information). The figure shows a wide distribution of the C1-C17 end-to-end distances (10.5 – 13.5 Å) with the micelle size indicating a wide different conformation of the SL alkyl chain in the aggregates. The $d_{C1\text{-}C17}$ are smaller than extended oleic acid chain length estimated to be below 26 Å in the "extended" conformation[106,107] indicating that the SL alkyl chain are bent with the COOH pointing toward the sophorose headgroup or slightly extended in the micelles. Similar observation was found by Prasad *et al.*[69] with acidic (three double bonds) linoleic acid sophorolipids.

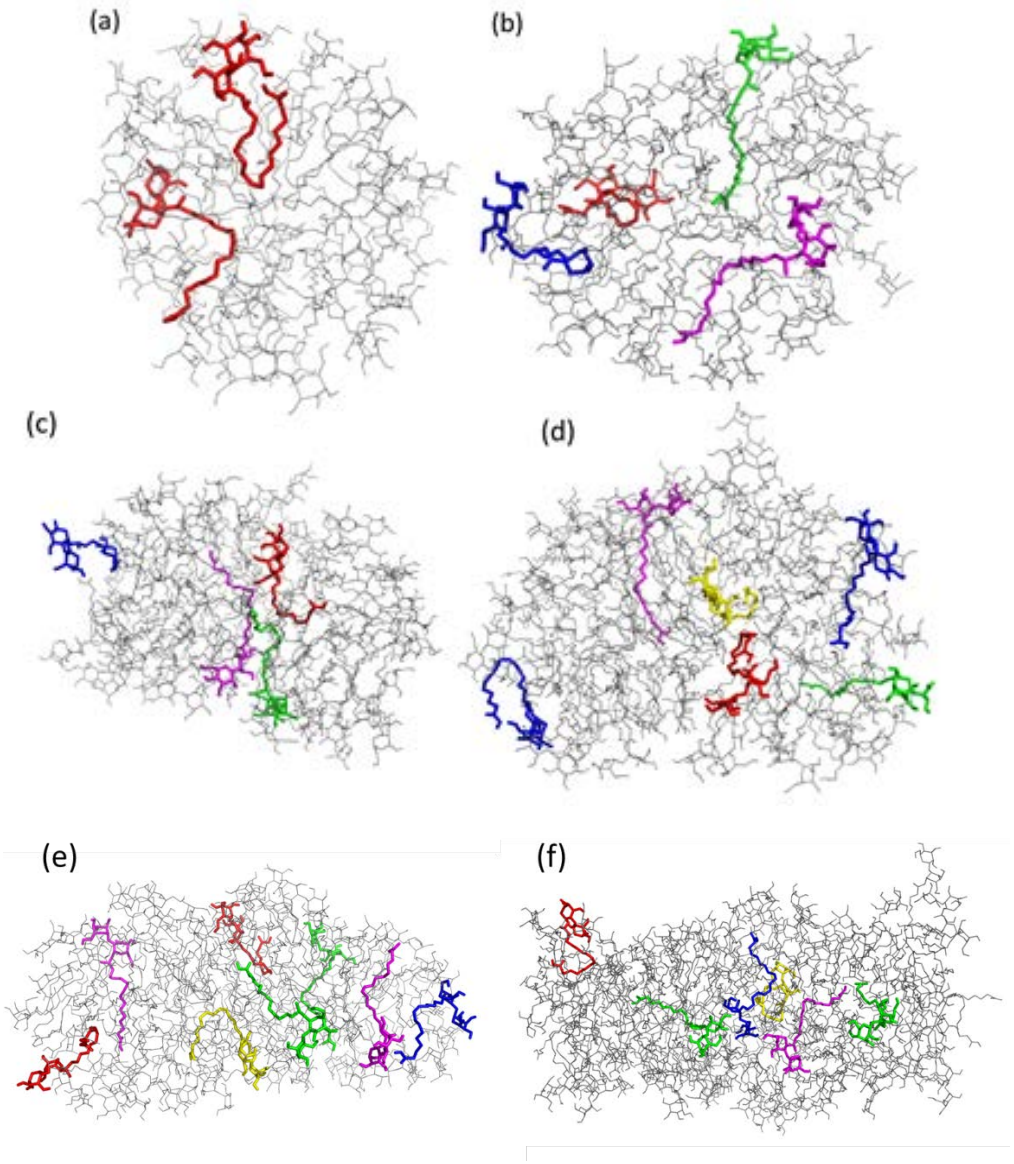

Figure 9 – Representative conformation of the sophorolipids in the aggregates with (a): 28, (b) 37, (c) 56, (d) 68 and (e) 80, (f) 112 monomers. Red, blue, green and yellow colours corresponds to the surfactant conformations where the sophorose and the COOH headgroups are located at the micelle surface with the rest of the surfactant in the hydrophobic core (red), the sophorolipid reside entirely at the micelle surface (blue), alkyl chain is extended and cross the hydrophobic core and with the sophorose and headgroups at the surface (magenta), where COOH in the hydrophobic core (green), where the overall sophorolipid are deeply buried in the hydrophobic core (yellow). The figures were drawn with PyMol.[100]

To illustrate this, we highlighted some representative conformations of the sophorolipids in each aggregate (Figure 9) according to their conformations and localizations and the model depicted in Figure 7. The Figures clearly show that the sophorolipid molecules adopt different conformations and localization in the micelles depending on their sizes. In particular, in the smallest micelle (N_{agg} = 28), which has a more spherical shape, there is only one

conformation (red-highlighted molecule in Figure (9(a-f) and region I in Figure 7) for the sophorolipid: the sophorose and the COOH headgroups are located at the micelle surface with the rest of the surfactant partially folded in the hydrophobic core. With the increase of the micelle size, the SL adopt other conformations, for instance, where the all the sophorolipid reside entirely at the micelle surface (blue-highlighted molecule in Figure 9(b-f) and region II in Figure 7), with the COOH in the hydrophobic core (green-highlighted molecule in Figure 9) or where the alkyl chain in an extended conformation that crosses the hydrophobic core and with the sophorose and headgroups at the surface (magenta-highlighted molecule in Figure 9(c-f) and region 3 in Figure 7)). In the aggregates with N_{agg} = 68, 80 and 112, we also see that one sophorolipid where the overall sophorolipid is buried in the hydrophobic core (yellow-highlighted molecule in Figure 9(d-f)). Taking together the simulation results show that for spherical micelles, the bent conformation of SL is predominant, but as soon as the shape turns into an ellipsoid, various conformations can coexist. These results also put in evidence the fact that the micelle is not constituted by a homogeneous arrangement of sophorose at the surface and oleic acid in the core, but rather a more complex distribution of these chemical groups, which is in agreement with the model picture proposed in Figure 7, deduced from experimental data. In particular, simulation data, both conformational and statistical, support the idea of a disordered region, which was identified as region II in Figure 7, in which molecular conformation and water interpenetration occur, thus explaining the complexity of fitting SAXS data using a standard core-shell model and justifying SANS contrast matching data showing that a pure aliphatic core only exists in the inner micellar center.

Conclusion

This work shows a detailed analysis of the micellar structure composed of sophorolipids, an asymmetric bolaform glycolipid containing a pH-sensitive COOH group. If the micellar structure was previously reported to be of prolate ellipsoidal shape, we show here how the asymmetric bolaform compound settles within the micelle itself. Detailed modelling of SAXS spectra show an uneven distribution of matter within the ellipsoid. We find that the core-shell model is by far the most adapted to describe the micelle; however, if the hydrophobic core, the size of which is about 8 x 55 Å, actually corresponds to an ellipsoidal shape, the hydrophilic shell has a non-zero thickness (about 12 Å) only in the equatorial region of the micelle. The actual micellar model rather corresponds to a “coffee bean” like shape than an actual homogeneous ellipsoid. Contrast matching SANS was used to probe the actual

distribution of the hydrophobic components of the micelle. The experiment was run at 100% D_2O, and at 46% D_2O, at which one expects sophorose to be fully contrasted. Interestingly, the hydrophobic core has rather a globular morphology, rather than an elongated ellipsoid. Combining both SAXS and SANS experiments, we make the hypothesis that the ellipsoid of revolution can be divided into three regions: Region I, defining a fully aliphatic core in the micellar center; a less-defined Region II in the axial direction of the ellipsoid and composed of aliphatic, sophorose and COOH groups; Region III, identifying the outer shell composed of sophorose, COOH groups, water and possibly counterions and in which contribution from vicinal CH_x groups should not be excluded. To account for such a complex structure, one must make the hypothesis that several configurations of sophorolipids are actually found within the micelle: both bent and elongated in the peripheral region but also crossing through the micelle itself. This picture is compatible with both the double polar nature of sophorolipids and the bent conformation of its oleic acid aliphatic chain.

To verify this model issued from experimental data, we carried out explicit MD simulations with 28, 37, 56, 68, 80 and 112 sophorolipid monomers. The simulation results show, in agreement, with scattering experiments, the micelle shape changes from a (quasi)sphere to an elongated ellipsoid that with the increase of the N_{agg} value. At high N_{agg} value (here, N_{agg}= 112 SL), the aggregate forms a cylindrical rod, as previously reported in the literature for higher volume fractions. Moreover, all the aggregates present rough surface with the sophorose and COOH headgroups in direct contact with the solvent leading to a larger hydration of these groups compared to the alkyl chain moiety. Examination of the sophorolipid conformations also shows that when the micelle is small and nearly spherical (here with N_{agg} = 28), the bent conformation of SL is predominant where the headgroup the sophorose and the COOH are located at the micelle surface with the alkyl chain partially folded in the hydrophobic core. With the increase of the micelle size, others SL conformations in the aggregate can coexist leading to a complex distribution of sophorolipids in the micelle surface and in a hydrophobic core, also in the agreement, with the model of structure deduced from the scattering experiments.

Finally, we have also investigated the sophorolipid configuration upon small increase in pH (< 7), when repulsive intermicellar interactions, due to the formation of COO^- groups, characterize the small angle scattering spectra and, consequently, the micellar network. To do so, we have employed anomalous SAXS, consisting into analyzing the sample using an X-ray incident energy close to the X-ray absorption edge of a given element, in this case Rb^+ (up to 100 mM) and Sr^{2+} (up to 20 mM) counterions, used to neutralize the negative COO^- charges.

Contrarily to our expectations, the ASAXS effect near the edge was very mild, if actually non existent, at concentrations in counterions at which it is supposed to be very strong, if we compared to ionic surfactant systems. We interpret these results by making the hypothesis that the negatively-charged COO^- groups do not preferably distribute at the outer micellar/water palisade but rather throughout the micellar hydrophilic shell volume, thus reducing the scattering effect of the counterions alone.

Acknowledgements

The research leading to these results has received funding from the European Community's Seventh Framework Programme (FP7/2007-2013) under Grant Agreement n° Biosurfing/289219. This work was, in part, granted access to the HPC resources of CCRT/CINES under the allocation x2014077322 (project number: gen7322) made by GENCI (Grand Equipement National de Calcul Intensif). SOLEIL Synchrotron (Saint Aubin, France) is kindly acknowledged for providing access to the SWING beamline.

Supporting Information Available

Page S1: Solvent SLD for all salt compositions. Page S2: Critical determination of the best fit model. Page S4: Fit parameters obtained for X_S= 0.3. Page S5: Molecular area values obtained for X_S= 0.3. Page S6: Experimental approach and data treatment in ASAXS experiments. Page S8: Experimental determination of the ionization degree. Page S9: Additional data obtained from molecular modelling by Molecular Dynamics. This information is available free of charge via the Internet at http://pubs.acs.org

References

[1] Tanford, C. The hydrophobic effect; Wiley: New York, 1973

[2] Imae, T.; Ikeda, S. Sphere-Rod Transition of Micelles of Tetradecyl-Trimethylammonium Halides in Aqueous Sodium Halide Solutions and Flexibility and Entanglement of Long Rodlike Micelles. *J. Phys. Chem*. **1986**, 90, 5216- 5223

[3] Lin, Z.; Cai, J. J.; Scriven, L. E.; Davis, H. T. Spherical-to-Wormlike Micelle Transition in CTAB Solutions *J. Phys. Chem*. **1994**, 98, 5984-5993

[4] Hayter, J. B.; Penfold J. Determination of Micelle Structure and Charge by Neutron Small-Angle Scattering, *Coll. Polymer Sci*. **1983**, 261, 1022-1030

[5] Goldmints, I.; von Gottberg, F. K.; Smith, K. A.; Hatton, T. A. Small-Angle Neutron Scattering Study of PEO−PPO−PEO Micelle Structure in the Unimer-to-Micelle Transition Region, *Langmuir* **1997**, 13, 3659–3664

[6] Fuhrhop, J. H.; Wang, T. Bolaamphiphiles, *Chem. Rev*. **2004**, 104, 2901-2937

[7] Bonini, M.; Berti, D.; Di Meglio, J. M.; Almgren, M.; Teixeira, J.; Baglioni, P. Surfactant Aggregates Hosting a Photoresponsive Amphiphile: Structure and Photoinduced Conformational Changes, *Soft Matter* **2005**, 1, 444–454

[8] Lu, T.; Han, F.; Mao, G.; Lin, G.; Huang, J.; Huang, X.; Wang, Y.; Fu, H. Effect of Hydrocarbon Parts of the Polar Headgroup on Surfactant Aggregates in Gemini and Bola Surfactant Solutions, *Langmuir* **2007**, 23, 2932-2936

[9] Douliez, J.-P. Self-Assembly of Hollow Cones in a Bola-amphiphile/Hexadiamine Salt Solution, *J. Am. Chem. Soc*. **2005**, 127, 15694-15695

[10] Sirieix, J.; Lauth-de Viguerie, N.; Rivière, M.; Lattes, A. From unsymmetrical bolaamphiphiles to supermolecules, *New J. Chem*. **2000**, 24, 1043-1048

[11] Kameta, N.; Masuda, M.; Minamikawa, H.; Shimizu, T. Self-Assembly and Thermal Phase Transition Behavior of Unsymmetrical Bolaamphiphiles Having Glucose- and Amino-Hydrophilic Headgroups, *Langmuir* **2007**, 23, 4634-4641

[12] Gubitosi, M.; Travaglini, L.; D'Annibale, A.; Pavel, N. V.; Tato, J. V.; Obiols-Rabasa, M.; Sennato, S.; Olsson, U.; Schillén, K.; Galantini, L. Sugar−Bile Acid-Based Bolaamphiphiles: From Scrolls to Monodisperse Single-Walled Tubules, *Langmuir* **2014**, 30, 6358−6366

[13] Fariya, M.; Jain, A.; Dhawan, V.; Shah, S.; Nagarsenker, M. S. Bolaamphiphiles: A Pharmaceutical Review, *Adv. Pharm. Bull*. **2014**, 4, 483-491

[14] Yan, Y.; Xiong, W.; Li, X.; Lu, T.; Huang, J.; Li, Z.; Fu H. Molecular Packing Parameter in Bolaamphiphile Solutions: Adjustment of Aggregate Morphology by Modifying the Solution Conditions, *J. Phys. Chem. B* **2007**, 111, 2225-2230

[15] Meister, A.; Bastrop, M.; Koschoreck, S.; Garamus, V. M.; Sinemus, T.; Hempel, G.; Drescher, S.; Dobner, B.; Richtering, W.; Huber, K.; Blume A. Structure-Property Relationship in Stimulus-Responsive Bolaamphiphile Hydrogels, *Langmuir* **2007**, 23, 7715-7723

[16] Caponetti, E.; Chillura-Martino, D.; La Mesa, C.; Muzzalupo, R.; Pedone, L. Structural and Transport Properties of Bola C-16 Micelles in Water and in Aqueous Electrolyte Solutions, *J. Phys. Chem. B* **2004**, 108, 1214-1223

[17] Muiioz, S.; Mallen, J.; Nakano, A.; Chen, Z.; Gay, I.; Echegoyen, L.; Gokel, G. W. Ultrathin Monolayer Lipid Membranes from a New Family of Crown Ether-Based Bola-Amphiphiles, *J. Am. Chem. Soc*. **1993**, 115, 1705-1711

[18] Garamus, V. M.; Milkereit, G.; Gerber, S.; Vill, V. Micellar Structure of a Sugar Based Bolaamphiphile in Pure Solution and Destabilizing Effects in Mixtures of Glycolipids, *Chem. Phys. Lett*. **2004**, 392, 105–109

[19] Davey, T. W.; Ducker, W. A.; Hayman, A. R. Aggregation of Omega-Hydroxy Quaternary Ammonium Bolaform Surfactants, *Langmuir* **2000**, 16, 2430-2435

[20] Shinde, N.; Narayan, K. S. Studies on Sodium Ricinoleate. 1. Adsorption and Aggregatlon Behavior, *J. Phys. Chem*. **1992**, 96, 5160-5165

[21] Nagarajan, R. Self-Assembly of Bola Amphiphiles, *Chem. Eng. Commun*. **1987**, 55, 251-273

[22] Menger, F. M.; Jerkunica, J. M.; Johnston, J. C. The Water Content of a Micelle Interior. The Fjord vs. Reef Models, *J. Am. Chem. Soc*. **1978**, 100, 4676-4678

[23] Brown, J. M.; Schofield, J. D. Localised Regions of Reduced Mobility in Micelles; 13C N.M.R. Spin-Lattice Relaxation Times of Functional Surfactants in Aqueous Solution, *J. Chem. Soc., Chem. Comm*. **1975**, 434

[24] Besnard, R.; Cambedouzou, J.; Arrachart, G.; Diat, O.; Pellet-Rostaing, S. Self-Assembly of Condensable "Bola-Amphiphiles" in Water/Tetraethoxysilane Mixtures for the Elaboration of Mesostructured Hybrid Materials, *Langmuir* **2013**, 29, 10368−10375

[25] Fu, D.-W.; Zhang, W.; Cai, H.-L.; Zhang, Y.; Ge, J.-Z.; Xiong, R.-G.; Huang, S. D. Supramolecular Bola-Like Ferroelectric: 4-Methoxyanilinium Tetrafluoroborate-18-crown-6, *J. Am. Chem. Soc*. **2011**, 133, 12780–12786

[26] Sano, M.; Oishi, K.; Ishi-i, T.; Shinkai, S. Vesicle Formation and Its Fractal Distribution by Bola-Amphiphilic [60]Fullerene, *Langmuir* **2000**, 16, 3773-3776

[27] Bai, S.; Debnath, S.; Javid, N.; Frederix, P. W. J. M.; Fleming, S.; Pappas, C.; Ulijn R. V. Differential Self-Assembly and Tunable Emission of Aromatic Peptide Bola-Amphiphiles Containing Perylene Bisimide in Polar Solvents Including Water, *Langmuir* **2014**, 30, 7576−7584

[28] Eggers, P. K.; Fyles, T. M.; Mitchell, K. D. D.; Sutherland T. Ion Channels from Linear and Branched Bola-Amphiphiles, *J. Org. Chem*. **2003**, 68, 1050-1058

[29] Ray, S.; Das, A. K.; Banerjee A. pH-Responsive, Bolaamphiphile-Based Smart Metallo-Hydrogels as Potential Dye-Adsorbing Agents, Water Purifier, and Vitamin B12 Carrier, *Chem. Mater*. **2007**, 19, 1633-1639

[30] Graf, G.; Drescher, S.; Meister, A.; Dobner, B.; Blume A. Self-Assembled Bolaamphiphile Fibers Have Intermediate Properties between Crystalline Nanofibers and Wormlike Micelles: Formation of Viscoelastic Hydrogels Switchable by Changes in pH and Salinity, *J. Phys. Chem. B* **2011**, 115, 10478–10487

[31] Van Bogaert, I. N. A.; Saerens, K.; De Muynck, C.; Develter, D.; Soetaert, W.; Vandamme, E. J. Microbial Production and Application of Sophorolipids, *Appl. Microbiol. Biotechnol*. **2007**, 76, 23–34

[32] Baccile, N.; Babonneau, F.; Jestin, J.; Pehau-Arnaudet, G.; Van Bogaert, I. N. A. Unusual, pH-Induced, Self-Assembly of Sophorolipid Biosurfactants, *ACS Nano* **2012**, 6, 4763–4776

[33] Baccile, N.; Pedersen, J. S.; Pehau-Arnaudet, G.; Van Bogaert, I. N. A. Surface Charge of Acidic Sophorolipid Micelles: Effect of Base and Time, *Soft Matter* **2013**, 9, 4911–4922
[34] Zhou, S.; Xu, C.; Wang, J.; Gao, W.; Akhverdiyeva, R.; Shah, V.; Gross, R. Supramolecular Assemblies of a Naturally Derived Sophorolipid, *Langmuir* **2004**, 20, 7926–7932
[35] Dhasaiyan, P.; Banerjee, A.; Visaveliya, N.; Prasad, B. L. V. Influence of the Sophorolipid Molecular Geometry on Their Self-Assembled Structures, *Chem. Asian J.* **2013**, 8, 369–372
[36] Penfold, J.; Chen, M.; Thomas, R. K.; Dong, C.; Smyth, T. J. P.; Perfumo, A.; Marchant, R.; Banat, I. M.; Stevenson, P.; Parry, A.; Tucker, I.; Grillo, I. Solution Self-Assembly of the Sophorolipid Biosurfactant and Its Mixture with Anionic Surfactant Sodium Dodecyl Benzene Sulfonate, *Langmuir* **2011**, 27, 8867-8877
[37] Develter, D. W. G.; Lauryssen, L. M. L. Properties and Industrial Applications of Sophorolipids, *Eur. J. Lipid Sci. Technol.* **2010**, 112, 628–638
[38] Maingault, M. Use of Sophorolipids and Cosmetic and Dermatological Compositions, WO/1995/034282A
[39] Singh, S.; Patel, P.; Jaiswal, S.; Prabhune, A. A.; Ramana, C. V.; Prasad, B. L. V. A Direct Method for the Preparation of Glycolipid–Metal Nanoparticle Conjugates: Sophorolipids as Reducing and Capping Agents for the Synthesis of Water Re-Dispersible Silver Nanoparticles and their Antibacterial Activity, *New J. Chem.* **2009**, 33, 646–652
[40] Sleiman, J. N.; Kohlhoff, S. A.; Roblin, P. M.; Wallner, S.; Gross, R.; Hammerschlag, M. R.; Zenilman, M. E.; Bluth, M. H. Sophorolipids as Antibacterial Agents, *Ann. Clin. Lab. Sci.* **2009**, 39, 60
[41] Fu, S. L.; Wallner, S. R.; Bowne, W. B.; Hagler, M. D.; Zenilman, M. E.; Gross, R.; Bluth, M. H. Sophorolipids and Their Derivatives are Lethal Against Human Pancreatic Cancer Cells, *J. Surg. Res.* **2008**, 148, 77-82
[42] Baccile, N.; Cuvier, A.-S.; Valotteau, C.; Van Bogaert, I. N. A. Practical Methods to Reduce Impurities for Gram-Scale Amounts of Acidic Sophorolipid Biosurfactants, *Eur. J. Lipid Sci. Technol.* **2013**, 115, 1404–1412
[43] Cuvier, A.-S.; Berton, J.; Stevens, C. V.; Fadda, G. C.; Babonneau, F.; Van Bogaert, I. N. A.; Soetaert, W.; Pehau-Arnaudet, G.; Baccile, N. pH-Triggered Formation of Nanoribbons From Yeast-Derived Glycolipid Biosurfactants, *Soft Matter*, **2014**, 10, 3950–3959
[44] http://www.sasview.org/
[45] http://danse.chem.utk.edu/downloads/ModelfuncDocs.pdf
[46] Marsh, D. Handbook of Lipid Bilayers, Second Edition, **2013**, p. 448
[47] Novotny, P.; Sohnel, O. Densities of Binary Aqueous Solutions of 306 Inorganic Substances, *J. Chem. Eng. Data* **1988**, 33, 49–55
[48] Hayter, J. B.; Penfold, J. An Analytic Structure Factor for Macroion Solutions, *Molec. Phys.* **1981**, 42, 109-118
[49] Hayter, J. B.; Penfold, J. A Rescaled MSA Structure Factor for Dilute Charged Colloidal Dispersions, *Molec. Phys.* **1982**, 46, 651-656
[50] Bales, B. L.; Zana, R. Characterization of Micelles of Quaternary Ammonium Surfactants as Reaction Media I: Dodeclytrimethylammonium Bromide and Chloride, *J. Phys. Chem. B* **2002**, 106, 1926-1939
[51] Berr, S. S.; Caponetti, E.; Johnson, J. S. (Jr.); Jones, R. R. M.; Magid, L. J. Small-Angle Neutron Scattering from Hexadecyltrimethylammonium Bromide Micelles in Aqueous Solutions, *J. Phys. Chem.* **1986**, 90, 22, 5666
[52] MacKerell, A. D. (Jr.) Molecular Dynamics Simulation Analysis of a Sodium Dodecyl Sulfate Micelle in Aqueous Solution: Decreased Fluidity of the Micelle Hydrocarbon Interior, *J. Phys. Chem.* **1995**, 99, 1846-1855
[53] Durchschlag, H.; Zipper, P. Calculation of the Partial Volume of Organic Compounds and Polymers *Progr. Colloid. Polym. Sci.* **1994**, 94, 20-39
[54] Cromer, D. T.; Liberman, D. A. Anomalous Dispersion Calculations Near to and on the Long-Wavelength Side of an Absorption Edge, *Acta Cryst.* **1981**, A37, 267-268
[55] http://ftp.esrf.fr/pub/scisoft/xop2.3/DabaxFiles/f1f2_BrennanCowan.dat
[56] Dreier, P.; Rabe, P.; Malzfeldt, W.; Niemann, W. Anomalous X-Ray Scattering Factors Calculated from Experimental Absorption Spectra, *J. Phys. C: Solid State Phys.* **1984**, 17, 3123-3136
[57] Patel, M.; Rosenfeldt, S.; Ballauff, M.; Dingenouts, N.; Pontoni, D.; Narayanan, T. Analysis of the Correlation of Counterions to Rod-Like Macroions by Anomalous Small-Angle X-Ray Scattering, *Phys. Chem. Chem. Phys.* **2004**, 6, 2962-2967
[58] Dingenouts, N.; Merkle, R.; Guo, X.; Narayanan, T.; Goerigk, G.; Ballauff, M. Use of Anomalous Small-Angle X-Ray Scattering for the Investigation of Highly Charged Colloids, *J. Appl. Cryst.* **2003**, 36, 578-582
[59] Guilleaume, B.; Blaul, J.; Ballauff, M.; Wittemann, M.; Rehahn, M.; Goerigk, G. The Distribution of Counterions Around Synthetic Rod-Like Polyelectrolytes in Solution, *Eur. Phys. J. E* **2002**, 8, 299–309
[60] Sztucki, M.; Di Cola, E.; Narayanan, T. Instrumental Developments for Anomalous Small-Angle X-Ray Scattering from Soft Matter Systems, *J. Appl. Cryst.* **2010**, 43, 1479–1487
[61] Ballauff, M.; Jusufi, A. Anomalous Small-Angle X-Ray Scattering: Analyzing Correlations and Fluctuations in Polyelectrolytes, *Colloid Polym. Sci.* **2006**, 284, 1303–1311

[62] Sztucki, M.; Di Cola, E.; Narayanan, T. Anomalous Small-Angle X-Ray Scattering from Charged Soft Matter, *Eur. Phys. J. Special Topics* **2012**, 208, 319–331
[63] Sztucki, M.; Di Cola, E.; Narayanan, T. New opportunities for Anomalous Small-Angle X-Ray Scattering to Characterize Charged Soft Matter Systems, *J. Phys.: Conf. Series* **2011**, 272, 012004
[64] Value obtained from the SciFinder® database
[65] Brulet, A.; Lairez, D.; Lapp, A.; Cotton, J.-P. Improvement of Data Treatment in Small-Angle Neutron Scattering, *J. Appl. Cryst*. 2007, 40, 165–177
[66] http://didier.lairez.fr/pasinet2/doku.php
[67] Hess, B.; Kutzner, C.; van der Spoel, D.; Lindahl, E. GROMACS 4: Algorithms for Highly Efficient, Load-Balanced, and Scalable Molecular Simulation. *J. Chem. Theory Comput*. **2008**, 4, 435–447
[68] Pronk, S.; Páll, S.; Schulz, R.; Larsson, P.; Bjelkmar, P.; Apostolov, R.; Shirts, M. R.; Smith, J. C.; Kasson, P. M.; van der Spoel, D.; *et al*. GROMACS 4.5: A High-Throughput and Highly Parallel Open Source Molecular Simulation Toolkit, *Bioinformatics* **2013**, 29, 845–854
[69] Dhasaiyan, P.; Pandey, P. R.; Visaveliya, N.; Roy, S.; Prasad, B. L. V. Vesicle Structures from Bolaamphiphilic Biosurfactants: Experimental and Molecular Dynamics Simulation Studies on the Effect of Unsaturation on Sophorolipid Self-Assemblies. *Chem. Europ J.* **2014**, 20, 6246–6250
[70] Oostenbrink, C.; Villa, A.; Mark, A. E.; van Gunsteren, W. F. A Biomolecular Force Field Based on the Free Enthalpy of Hydration and Solvation: The GROMOS Force-Field Parameter Sets 53A5 and 53A6, *J. Comput. Chem.* **2004**, 25, 1656–1676
[71] Hansen, H. S.; Hünenberger, P. H. A Reoptimized GROMOS Force Field for Hexopyranose-Based Carbohydrates Accounting for the Relative Free Energies of Ring Conformers, Anomers, Epimers, Hydroxymethyl Rotamers, and Glycosidic Linkage Conformers. *J. Comput. Chem*. **2011**, 32, 998–1032
[72] Kukol, A. Lipid Models for United-Atom Molecular Dynamics Simulations of Proteins. *J. Chem. Theory Comput*. **2009**, 5, 615–626
[73] Berendsen, H. J. C.; Postma, J. P. M.; van Gunsteren, W. F. Intermolecular Forces; Pullman, B. Ed.: Reidel Dodrecht, **1981**; p. 331
[74] Miyamoto, S.;; Kollman, P. A. Settle: An Analytical Version of the SHAKE and RATTLE Algorithm for Rigid Water Models, *J. Comput. Chem*. **1992**, 13, 952–962
[75] Bussi, G.; Donadio, D.; Parrinello, M. Canonical Sampling through Velocity Rescaling. *J. Chem. Phys*. **2007**, 126, 014101
[76] Rahman, A.; Stillinger, F. H. Molecular Dynamics Study of Liquid Water, *J. Chem. Phys.* **1971**, 55, 3336–3359
[77] Parrinello, M. Polymorphic Transitions in Single Crystals: A New Molecular Dynamics Method, *J. Appl. Phys*. **1981**, 52, 7182–7190
[78] Hess, B. P-LINCS: A Parallel Linear Constraint Solver for Molecular Simulation. *J. Chem. Theory Comput*. **2007**, 4, 116–122
[79] Tironi, I. G.; Sperb, R.; Smith, P. E.; van Gunsteren, W. F. A Generalized Reaction Field Method for Molecular Dynamics Simulations. *J. Chem. Phys.* **1995**, 102, 5451
[80] Heinz, T. N.; van Gunsteren, W. F.; Hu̇nenberger, P. H. Comparison of Four Methods to Compute the Dielectric Permittivity of Liquids from Molecular Dynamics Simulations. *J. Chem. Phys*. **2001**, 115, 1125
[81] Water and Biomolecules: Physical Chemistry of Life Phenomena, Kuwajima, K.; Goto, Y.; Hirata, F.; Terazima, M.; Kataoka, M. Eds., Springer-Verlag, Berlin Heidelberg, **2009**, p.221.
[82] Advances in Sweeteners, Grenby, T. H. Ed., Blackie Academics and Professionals, Glasgow, **1996**, p.192
[83] Dupuy, C.; Auvray, X.; Petipas, C.; Rico-Lattes, I.; Lattes, A. Anomeric Effects on the Structure of Micelles of Alkyl Maltosides in Water, *Langmuir* **1997**, 13, 3965-3967
[84] Abel, S.; Dupradeau, F.-Y.; Raman, E. P.; MacKerell, A. D. (Jr.); Marchi, M. Molecular Simulations of Dodecyl-β-maltoside Micelles in Water: Influence of the Headgroup Conformation and Force Field Parameters, *J. Phys. Chem. B*. **2011**, 115, 487–499
[85] Lupi, L.; Comez, L.; Paolantoni, M.; Perticaroli, S.; Sassi, P.; Morresi, A.; Ladanyi, B. M.; Fioretto, D. Hydration and Aggregation in Mono- and Disaccharide Aqueous Solutions by Gigahertz-to-Terahertz Light Scattering and Molecular Dynamics Simulations, *J. Phys. Chem. B* **2012**, 116, 14760−14767
[86] Winther, L. R.; Qvist, J.; Halle, B. Hydration and Mobility of Trehalose in Aqueous Solution, *J. Phys. Chem. B* **2012**, 116, 9196−9207.
[87] Glinski, J.; Burakowski, A. Is the Hydration Number of a Non-Electrolyte Additive With Length and Constituents of The Solute Molecule?, *Eur. Phys. J. Special Topics* **2008**, 154, 275–279
[88] Mähler, J.; Persson, I.; A Study of the Hydration of the Alkali Metal Ions in Aqueous Solution, *Inorg. Chem*. **2012**, 51, 425–438
[89] Moreau, G.; Helm, L.; Purans, J.; Merbach, A. E. Structural Investigation of the Aqueous Eu2+ Ion: Comparison with Sr2+ Using the XAFS Technique, *J. Phys. Chem. A* **2002**, 106, 3034-3043

[90] Zini, E.; Gazzano, M.; Scandola, M.; Wallner, S. R.; Gross, R. A. Glycolipid biomaterials: Solid-state properties of a poly(sophorolipid), *Macromolecules* **2008**, 42, 7463-7468
[91] Cecutti, C.; Focher, B.; Perly, B.; Zemb, T. Glycolipid Self-Assembly: Micellar Structure, *Langmuir* **1991**,7, 2580-2585
[92] Chen, M.; Dong, C.; Penfold, J.; Thomas, R. K.; Smyth, T. J. P.; Perfumo, A.; Marchant, R.; Banat, I. M.; Stevenson, P.; Parry, A.; Tucker, I.; Campbell, R. A. Adsorption of Sophorolipid Biosurfactants on Their Own and Mixed with Sodium Dodecyl Benzene Sulfonate, at the Air/Water Interface *Langmuir* **2011**, 27, 8854–8866
[93] Pabit, S. A.; Meisburger, S. P.; Li, L.; Blose, J. M.; Jones, C. D.; Pollack, L. Counting Ions Around DNA with ASAXS, *J. Am. Chem. Soc*. **2010**, 132, 16334–16336
[94] Huber, K.; Scheler, U. New experiments for the quantification of counterion condensation, Curr. Op. Coll. Interf. Sci., 2012, 17, 64–73
[95] Jusufi, A.; Kohlmeyer, A.; Sztucki, M.; Narayanan, T.; Ballauff, M. Self-Assembly of Charged Surfactants: Full Comparison of Molecular Simulations and Scattering Experiments, *Langmuir* **2012**, 28, 17632−17641
[96] Glatter, O. A New Method for the Evaluation of Small-Angle Scattering Data, *J. Appl. Cryst*. **1977**, 10, 415
[97] Gerber, S.; Garamus, V. M.; Milkereit, G.; Vill V. Mixed Micelles Formed by SDS and a Bolaamphiphile with Carbohydrate Headgroups, *Langmuir* **2005**, 21, 6707-6711
[98] Milkereit, G. Investigation of colloidal, biophysical and liquid crystalline properties of synthetic alkyl glycosides and glycolipids, PhD thesis, **2006**, University of Hamburg, Germany (http://www.chemie.uni-hamburg.de/bibliothek/2006/DissertationMilkereit.pdf)
[99] Abel, S.; Dupradeau, F.-Y.; Marchi, M. Molecular Dynamics Simulations of a Characteristic DPC Micelle in Water. J. *Chem. Theory Comput*. **2012**, 8, 4610–4623
[100] Schrodinger, L. The PyMOL Molecular Graphics System. DeLano Scientific San Carlos CA, 2010
[101] Baccile, N.; Nassif, N.; Malfatti, L.; Van Bogaert, I. N. A.; Soetaert, W.; Pehau-Arnaudet, G.; Babonneau, F. Sophorolipids: A Yeast-Derived Glycolipid as Greener Structure Directing Agents for Self-Assembled Nanomaterials, *Green Chem*. **2010**, 12, 1564-1567
[102] Abel, S.; Sterpone, F.; Bandyopadhyay, S.; Marchi, M. Molecular Modeling and Simulations of AOT−Water Reverse Micelles in Isooctane: Structural and Dynamic Properties, *J. Phys. Chem. B* **2004**, 108, 19458–19466
[103] Voronoi, G. F. Nouvelles Applications des Paramètres Continus à la Théorie des Formes Quadratiques. *J. Reine Angew. Math*. **1908**, 134, 198–287
[104] Rycroft, C. H. VORO++: A Three-Dimensional Voronoi Cell Library in C++, *Chaos* **2009**, 19, 041111
[105] Paci, E.; Marchi, M. Intrinsic Compressibility and Volume Compression in Solvated Proteins by Molecular Dynamics Simulation at High Pressure. *Proc. Natl. Acad. Sci. U. S. A*. **1996**, 93, 11609–11614
[106] Kaibara, K.; Iwata, E.; Eguchi, Y.; Suzuki, M.; Maeda, H. Dispersion Behavior of Oleic Acid in Aqueous Media: from Micelles to Emulsions, *Colloid Polym. Sci* **1997**, 275, 777-783
[107] Garland, E. R.; Rosen, E. P.; Clarke, L. I.; Baer, T. Structure of Submonolayer Oleic Acid Coverages on Inorganic Aerosol Particles: Evidence of Island Formation, *Phys. Chem. Chem. Phys*. **2008**, 10, 3156-3161